Equation of state for a partially ionized gas. II

George A. Baker, Jr.
Theoretical Division, Los Alamos National Laboratory, University of California, Los Alamos, New Mexico 87544, USA
(Received 27 March 2003; revised manuscript received 16 May 2003; published 20 November 2003)

The derivation of equations of state for fluid phases of a partially ionized gas or plasma is addressed from a fundamental point of view. A spherical cellular model is deduced for the hot curve limit (or ideal Fermi gas). Next the Coulomb interactions are added to the spherical cellular model for general ionic charge *Z*. Then an independent electron model within a *Z* electron cell plus several many-body effects are employed. Numerical examples of the theory for several elements (H, Li, N, Na, K, Ni, Rb, Pd, Cs, and Er) are reported. These results reduce in various limits of temperature and density to the expected behavior. They display electron, localization-delocalization phase transitions of liquid-gas character. In the higher *Z* elements, a second possible critical point has been found. The critical pressure, electron density and temperature for the lower-density critical points seem to obey power laws as a function of *Z*.

DOI: 10.1103/PhysRevE.68.056112 PACS number(s): 05.30.−d, 51.30.+i, 05.70.Ce, 64.10.+h

I. INTRODUCTION AND SUMMARY

While the theory of crystalline solids has been very well developed, the properties of fluids and amorphous solids considered at the level of the quantum mechanics of electrons and ions have received much less attention. For crystalline solids Bloch's theorem is frequently relied upon to provide the general structure of the necessary quantum mechanical wave functions. A study at the level of the quantum mechanics of ions and electrons was begun in a previous paper [1]. In that paper quantum statistical mechanics was used to develop a theory of a cellular model of a fluid. It was the purpose of that paper to begin to construct a fundamental investigation of a partially ionized gas. Of course, there is not any firm dividing line between either a partially ionized gas and a fully ionized gas, or a nonionized fluid. In that paper the numerical evaluations of the theory were limited to hydrogen. It is the purpose of the present paper to investigate elements with more than one electron per atom. My results have many of the expected physical properties. In the low-density limit at fixed temperature full ionization is seen. At medium to high density, there is a density dependent temperature below which the pressure is very insensitive to the temperature.

There are a number of other approaches to this problem which are worthy of mention. Perhaps the most generally used theories are the semiclassical theories of Thomas and Fermi [2–7] and their Thomas-Fermi-Dirac generalization to include the exchange interaction [8–10]. Further approaches are mentioned in Ref. [1].

In Sec. II, I briefly recall the framework developed in Ref. [1]. I set out the quantum statistical mechanical formalism for fermionic electrons and Maxwell-Boltzmann ions. The Helmholtz free energy is derived and from it the pressure and the internal energy are derived in the standard manner. One different feature is the appearance of the partial of the energy eigenvalues with respect to the temperature in the formula for the energy. This term occurs because the self-consistent potential depends on the temperature. The true physical interactions of course do not. The equations for the case of Z electrons and an ion of charge $+Ze$ are given.

In Sec. III, I simplify the formulation described in the preceding section by the introduction of an independent electron approximation inside the cell. The modification of the size of the spherical cell for this approximation is discussed. The numerical accuracy requirements are also discussed. I give expressions for the necessary derivatives with respect to the temperature and the radius of the spherical cell. The method for the computation of the self-consistent potential is described.

In Sec. IV, I report the results of the computation for the spherical cellular model in the high- and low-density regimes. The expected temperature independence for high densities and moderate temperatures is shown. Likewise the Gibbs free energy μ is found to be proportional to the two-thirds power of the density in the high-density limit, as expected. In this limit, the pressure for the spherical cellular model is seen to be lower than that for the Thomas-Fermi model. I have studied the deviations from the low-temperature limit in the high-density region. I find that the deviations are proportional to $\zeta^{-2/3}y^{-8}$ instead of just $\zeta^{-2/3}$ as expected. Here ζ is the de Broglie density, Eq. (2.9), and y^2 is the ratio of the Coulomb energy to the thermal energy Eq. (2.9). The small y limit is built into the model and the deviations from the ideal gas are proportional to y^2. For low densities the coefficient of this term tends to zero and a y^3 term is predicted by the exact theory [11], but only very rough agreement is seen.

In Sec. V, I report the numerical results for intermediate densities. Here I find critical points and phase boundaries. These features either indicate limits on the validity of the model or possible plasma phase transitions. Various critical points are reported for a sample of ten elements. The critical-point values of the pressure, electron density, and temperature more or less obey power laws as a function of the ionic charge Z. The plot of all the phase boundaries in the ζ-y plane seems to show (except for hydrogen) a universal boundary for the one-phase regions. There does not appear to be (again except for hydrogen) any two-phase regions for small de Broglie density. I plot some examples of the spherical cellular model's internal energy and its ''physically reasonable'' energy, Eq. (5.2).

In Appendix A, I give the results of long computations which are required to evaluate the derivatives.

Finally, in Appendix B, for the convenience of the reader, I give a list of the many approximations which are made in the spherical cellular model as implemented in this paper.

II. FORMULATION OF THE CELLULAR MODEL

Before reviewing the formulation of the cellular model, it is worthwhile to quote briefly the necessary quantum statistical mechanical formulas that I will need. I will make the Born-Oppenheimer separation and will treat the electrons as fermions, but only treat the ions as Maxwell-Boltzmann particles. I will need the pressure and the energy of an atom enclosed in a cell. I will suppose that the nucleus is fixed in the center of the cell. The most straightforward thing to compute is the grand canonical partition function which is normally given as [12]

$$\begin{aligned}\mathcal{Q}(\Omega,T)&=\sum_{\mathcal{N}=0}\exp[\mathcal{N}\mu(\Omega,T)/(kT)]Q_{\mathcal{N}}(\Omega,T)\\&=\sum_{\mathcal{N}=0}^{\infty}\sum_{\substack{\{n_j\}\\ \Sigma n_j=\mathcal{N}}}\exp\{[\mu(\Omega,T)-\epsilon_j]n_j/(kT)\}\\&=\prod_j\,(1+\exp\{[\mu(\Omega,T)-\epsilon_j]/(kT)\}),\end{aligned}\tag{2.1}$$

for the case of Fermi statistics. By taking the partial derivative of $\ln\mathcal{Q}$ with respect to the parameter μ, I can obtain in the usual manner,

$$\mathcal{N}=\sum_j\frac{1}{\exp[(\epsilon_j-\mu)/kT]+1},\tag{2.2}$$

where $\mathcal{N}$ is the average number of occupied states of the system. Equation (2.2) fixes μ, as a function of the temperature and the volume. For the canonical partition function $Q_{\mathcal{N}}(\Omega,T)$, as usual I have $kT\ln Q_{\mathcal{N}}=-A(\Omega,T)$. $A(\Omega,T)$ is the Helmholtz free energy. I deduce directly from Eq. (2.1) in the usual way by considering only the term in the sum corresponding to $\mathcal{N}$,

$$\begin{aligned}A(\Omega,T)&=\mathcal{N}\mu(\Omega,T)\\&\quad-kT\sum_j\,\ln(1+\exp\{[\mu(\Omega,T)-\epsilon_j]/(kT)\}).\end{aligned}\tag{2.3}$$

The internal energy is given from the Helmholtz free energy by the thermodynamic relation

$$U=A-T\left.\frac{\partial A}{\partial T}\right|_{\Omega}=\sum_j\frac{\epsilon_j-T\left.\dfrac{\partial\epsilon_j}{\partial T}\right|_{\Omega}}{\exp[(\epsilon_j-\mu)/kT]+1}.\tag{2.4}$$

I remark that normally, $\partial\epsilon_j/\partial T|_{\Omega}=0$ and so is not included in the text book presentations. However, in my case, my treatment of the many-body effects induces a temperature dependence in energy eigenvalues in the cellular equations. The term $\partial\epsilon_j/\partial T|_{\Omega}$ is not always small and leads to some interesting behavior as is discussed in Sec. V. The pressure is also given from the Helmholtz free energy by the thermodynamic relation

$$\begin{aligned}p&=-\left.\frac{\partial A}{\partial\Omega}\right|_T\\&=\sum_j\frac{\left.\dfrac{\partial\mu}{\partial\Omega}\right|_T-\left.\dfrac{\partial\epsilon_j}{\partial\Omega}\right|_T}{\exp[(\epsilon_j-\mu)/kT]+1}-\mathcal{N}\left.\frac{\partial\mu}{\partial\Omega}\right|_T,\\&=-\sum_j\frac{\left.\dfrac{\partial\epsilon_j}{\partial\Omega}\right|_T}{\exp[(\epsilon_j-\mu)/kT]+1}.\end{aligned}\tag{2.5}$$

It will be useful to rewrite Eq. (2.5) in terms of the "radius" r_b, or typical linear dimension of the cell as

$$p\Omega=-\frac{1}{3}\sum_j\frac{r_b\left.\dfrac{\partial\epsilon_j}{\partial r_b}\right|_T}{\exp[(\epsilon_j-\mu)/kT]+1}.\tag{2.6}$$

The subscript j is a general dummy index and will be replaced later by the more specific l,λ, etc.

For the case of the ideal Fermi gas, Baker showed in Ref. [1] that if one divides space up into a simple cubic lattice structure (or any Bravais lattice for that matter) with an average of one Fermion per unit cell, then the appropriate solution in the individual cell is identical to the exact solution for the ideal Fermi gas. Briefly, the discussion is as follows. Bloch's theorem on crystal lattices [13] says that any solution for the "one-electron wave function" is of the form $\psi(\vec{r})=e^{i\vec{k}\cdot\vec{r}}\phi(\vec{r})$, where $\phi(\vec{r})$ has the periodicity of the lattice. By using all the $\vec{k}$ which lie in the first Brillouin zone, one can construct the entire band corresponding to that state. By the general theory the combination of all the reciprocal lattice vectors plus those in the first Brillouin zone covers the entire $\vec{k}$ space. Here the boundary conditions are

$$\psi(\vec{r})=e^{-i\vec{k}\cdot\vec{R}}\psi(\vec{r}+\vec{R})\tag{2.7}$$

and

$$\vec{n}(\vec{r})\cdot\vec{\nabla}\psi(\vec{r})=-e^{-i\vec{k}\cdot\vec{R}}\vec{n}(\vec{r}+\vec{R})\cdot\vec{\nabla}\psi(\vec{r}+\vec{R}),$$

or

$$\vec{n}(\vec{r})\cdot\vec{\nabla}\phi(\vec{r})=-\vec{n}(\vec{r}+\vec{R})\cdot\vec{\nabla}\phi(\vec{r}+\vec{R}),\tag{2.8}$$

where $\vec{n}(\vec{r})$ is the outward normal vector to the surface of the cell and $\vec{R}$ is a lattice vector. These conditions provide for the continuity of the wave function and its derivative at the surface of the cell. From my point of view, every calculation I make must be reduced to a single cell and the macroscopic effects are reflected solely through the boundary conditions, and the effective mass and potential modifications.

The standard formulas [12] for the ideal electron gas are

$$f_n(z)=\frac{1}{\Gamma(n)}\int_0^\infty \frac{z\,\eta^{n-1}e^{-\eta}d\eta}{1+ze^{-\eta}},\quad \frac{4\pi r_b^3}{3}=\frac{\Omega}{N},$$

$$\zeta=\frac{ZN}{2\Omega}\left(\frac{h^2}{2\pi mkT}\right)^{3/2}=f_{3/2}(z),$$

$$\frac{p\Omega}{NkT}=\frac{f_{5/2}(z)}{f_{3/2}(z)},\quad y^2=\frac{Ze^2}{r_bkT},\quad p\Omega=\frac{2}{3}U, \tag{2.9}$$

where ζ is the de Broglie density which measures the importance of quantum effects, N is the number of electrons, Ω is the volume, m is the electron mass, and $z=\exp(\mu/kT)$ in the notation of Eq. (2.2). The quantity y measures the ratio of the Coulomb energy to the thermal energy, and U is the internal energy.

The next step in the development of the cellular model is to approximate the cell shape by a sphere. Since one cannot fill space with spheres of a uniform size, I choose the size of the spherical cell to be such that it has the average volume occupied by a single fermion. The Schrödinger equation separates in the usual spherical coordinates r,θ, and ϕ. The eigenfunctions are the spherical Bessel functions $j_l(p_{l,\lambda}r)$, the Legendre polynomials $P_l(\cos\theta)$, and the exponentials $\exp(im\phi)$, where l and m are integers and i is the square root of -1. I impose the boundary conditions of periodicity in all directions, i.e., at every point of the surface, which ensures the continuity of the wave function and its derivative for two such spheres in contact.

Baker [1] has given the following generalization for the case of a cell with a $+Ze$ charged nucleus and Z electrons. The Schrödinger equation for this cellular model is

$$\sum_{j=1}^{Z}\left\{\frac{\hbar^2}{2m^*}[k^2-2i\vec{k}\cdot\vec{\nabla}_j-\nabla_j^2]-\frac{Ze^2}{r_j}+\frac{3Ze^2}{10r_b}g(y^2)\right\}\phi_\lambda(\vec{r}_1,\ldots,\vec{r}_Z)+\left\{\frac{1}{2}\sum_{j\neq l}^{Z}\frac{e^2}{|\vec{r}_l-\vec{r}_j|}+\frac{3e^2}{2r_b}F\left(\frac{y^2}{Z}\right)\left[Z-\frac{1}{3}\sum_{j=1}^{Z}\left(\frac{r_j}{r_b}\right)^2\right.\right.$$
$$\left.\left.-\frac{4}{3}Z\left(\frac{3Z}{\pi\zeta}\right)^{1/3}f_{1/2}(z(\zeta))\right]\right\}\phi_\lambda(\vec{r}_1,\ldots,\vec{r}_Z)+\frac{6Z^2e^2}{5r_b}F(y^2Z)\phi_\lambda(\vec{r}_1,\ldots,\vec{r}_Z)$$
$$=E_\lambda(\vec{k})\phi_\lambda(\vec{r}_1,\ldots,\vec{r}_Z), \tag{2.10}$$

where $m^*/m=1$ and the $f_{1/2}$ term is dropped for the antiparallel spin case. Here m^* is given by

$$\frac{m}{m^*}=1+A(\zeta)\frac{y^2}{Z}F\left(\frac{y^2}{Z}\right),$$

$$A(\zeta)=\frac{2}{3}\left(\frac{\zeta}{Z}\right)^{2/3}\left(\frac{3}{\pi}\right)^{1/3}\left\{\frac{2f_{1/2}(z(\zeta))-X(\zeta)/(\pi\zeta)}{f_{5/2}(z(\zeta))}\right\}. \tag{2.11}$$

This result is arrived at by starting with the Heitler-London equation which is valid in the cold, dilute limit and by adding corrections, proportional to F and g. In the cold dilute limit, $F=g=0$. When $F=g=1$, the equation is correct for the hot, ideal-gas limit through order y^2. The functions F and g vary monotonically between 1 and 0 as y varies between 0 and ∞. Baker in Sec. V of Ref. [1] has given a semiclassical derivation of these many-body terms. He also derived the effective mass terms of Eq. (2.11) as part of the exchange correction. The derivation of $X(\zeta)$ is to be found in Ref. [14].

I separate out the state independent terms

$$\mathcal{E}_{l,\lambda}=E_{l,\lambda}+\Delta E_{\|\text{ or anti-}\|}, \tag{2.12}$$

where

$$\Delta E_{\|}=-\frac{3Ze^2}{10r_b}g(y^2)-\frac{3Ze^2}{2r_b}F\left(\frac{y^2}{Z}\right)\times\left[1-\frac{4}{3}\left(\frac{3Z}{\pi\zeta}\right)^{1/3}f_{1/2}(z(\zeta))\right]-\frac{6Z^2e^2}{5r_b}F(y^2Z),$$

$$\Delta E_{\text{anti-}\|}=-\frac{3Ze^2}{10r_b}g(y^2)-\frac{3Ze^2}{2r_b}F\left(\frac{y^2}{Z}\right)-\frac{6Z^2e^2}{5r_b}F(y^2Z). \tag{2.13}$$

Equation (2.10) simplifies to

$$\sum_{j=1}^{Z}\left\{\frac{\hbar^2}{2m^*}[k^2-2i\vec{k}\cdot\vec{\nabla}_j-\nabla_j^2]-\frac{Ze^2}{r_j}\right\}\phi_{l,\lambda}(\vec{r}_1,\ldots,\vec{r}_Z)+\left\{\frac{1}{2}\sum_{j\neq l}^{Z}\frac{e^2}{|\vec{r}_l-\vec{r}_j|}-\frac{e^2}{2r_b}F\left(\frac{y^2}{Z}\right)\sum_{j=1}^{Z}\left(\frac{r_j}{r_b}\right)^2\right\}$$
$$\times\phi_{l,\lambda}(\vec{r}_1,\ldots,\vec{r}_Z)=\mathcal{E}_{l,\lambda}(\vec{k})\phi_\lambda(\vec{r}_1,\ldots,\vec{r}_Z), \tag{2.14}$$

where $m^*/m=1$ for the antiparallel case.

The generalized expression for $\epsilon_{l,\lambda}(\vec{k})$ is

$$\epsilon_{l,\lambda}(\vec{k})=\frac{1}{2}\left(1+\frac{m^*}{m}\right)\mathcal{E}_{l,\lambda}(\vec{k})+\frac{3Ze^2}{10r_b}g(y^2)+\frac{3Z^2e^2}{5r_b}F(y^2Z)$$
$$-\frac{1}{2}\left(1-\frac{m^*}{m}\right)\langle\phi_{l,\lambda}|\sum_{j=1}^{Z}\frac{Ze^2}{r_j}-\frac{1}{2}$$
$$\times\sum_{j\neq l}\frac{e^2}{|\vec{r}_j-\vec{r}_l|}|\phi_{l,\lambda}\rangle+\frac{e^2}{r_b}F\left(\frac{y^2}{Z}\right)$$
$$\times\left[\frac{3}{4}Z+\frac{m^*}{4m}\sum_{j=1}^{Z}\langle\phi_{l,\lambda}|\frac{r_j^2}{r_b^2}|\phi_{l,\lambda}\rangle-Z\left(\frac{3Z}{\pi\zeta}\right)^{1/3}\right.$$
$$\left.\times f_{1/2}(z(\zeta))\right]. \tag{2.15}$$

For the antiparallel case, $m^*/m=1$ and the $f_{1/2}$ term is dropped.

III. INDEPENDENT ELECTRON MODEL OF THE Z ELECTRON CELL

Since the Z electron model is currently intractable, I consider the simplification of using ''independent electrons.'' The first step, as was done by Hartree, is to use the form of the wave function, $\phi_\lambda(\vec{r}_1,\ldots,\vec{r}_Z)=\Pi_{i=1}^{Z}\phi_i(\vec{r}_i)$. In Eq. (2.14) all the terms except the electron-electron interaction can be neatly divided so as to depend on the single-vector variable $\vec{r}_i$ alone. By the method of the separation of variables, the equation for each single electron can be obtained by integration over the other electrons of the electron-electron interaction terms. Of course, as is well known, this leads to a complex self-consistency problem. Instead, I will also impose the condition of a single, temperature and density dependent, self-consistent charge density. With these conditions I propose, instead of Eq. (2.14), the equation,

$$\left\{\frac{\hbar^2}{2m^*}[k^2-2i\vec{k}\cdot\vec{\nabla}-\nabla^2]-\frac{e^2v(r_b,T,r/r_b)}{r}\right.$$
$$\left.-\frac{e^2}{2r_b}\left(\frac{r}{r_b}\right)^2F\left(\frac{y^2}{Z}\right)\right\}\phi_{l,\lambda}(\vec{r})=\tilde{\mathcal{E}}_{l,\lambda}(\vec{k})\phi_{l,\lambda}(\vec{r}). \tag{3.1}$$

The potential $e^2v(r_b,T,r/r_b)/r$ is composed of two parts. The first is the electron-ion interaction which is just Ze^2/r as seen in Eq. (2.14). The second part is a representation of the electron-electron interaction. Since I want to have the full ion potential at the origin I select $v(r_b,T,0)=Z$. Since an electron does not screen itself, I want to see the potential of only a single ionic charge at the cellular surface, so I select $v(r_b,T,1)=1$. It is important to note however that, when I add up all the energies, I will have counted $Z(Z-1)$ terms, when, as we saw in Eq. (2.14), I should have only $\frac{1}{2}Z(Z-1)$ such terms. In the computation of the ϵ's I must therefore subtract the extra terms off. The electron-electron repulsion is given by

$$\frac{Ze^2}{r}-\frac{e^2v(r_b,T,r/r_b)}{r}. \tag{3.2}$$

Thus for the corresponding ϵ,

$$\epsilon_{l,\lambda}(\vec{k})=\frac{1}{2}\left(1+\frac{m^*}{m}\right)\left[\tilde{\mathcal{E}}_{l,\lambda}(\vec{k})-\frac{1}{2}\langle\phi_{l,\lambda}(\vec{r})|\right.$$
$$\left.\times\left(\frac{Ze^2}{r}-\frac{e^2v(r_b,T,r/r_b)}{r}\right)|\phi_{l,\lambda}(\vec{r})\rangle\right]$$
$$-\frac{1}{2}\left(1-\frac{m*}{m}\right)\langle\phi_{l,\lambda}(\vec{r})|\frac{v(r_b,T,r/r_b)e^2}{r}|\phi_{l,\lambda}(\vec{r})\rangle$$
$$+\frac{m^*e^2}{4mr_b}F\left(\frac{y^2}{Z}\right)\langle\phi_{l,\lambda}(\vec{r})|\frac{r^2}{r_b^2}|\phi_{l,\lambda}(\vec{r})\rangle+\Delta\epsilon_{\|\text{ or anti-}\|}, \tag{3.3}$$

where the state independent part is

$$\Delta\epsilon_{||}=\frac{3e^2}{10r_b}g(y^2)+\frac{3Ze^2}{5r_b}F(y^2Z)$$
$$+\frac{e^2}{r_b}F\left(\frac{y^2}{Z}\right)\left[\frac{3}{4}-\left(\frac{3Z}{\pi\zeta}\right)^{1/3}f_{1/2}(z(\zeta))\right],$$
$$\Delta\epsilon_{\text{anti-}||}=\frac{3e^2}{10r_b}g(y^2)+\frac{3Ze^2}{5r_b}F(y^2Z)+\frac{3e^2}{4r_b}F\left(\frac{y^2}{Z}\right). \tag{3.4}$$

Again, for the antiparallel case $m^*/m=1$ and I drop the $f_{1/2}$ term. The modifications to take account of the exchange and many-body effects are included.

At this point, a technical complication arises. That is the treatment of the term $\hat{H}=-(i\hbar^2/m)\vec{k}\cdot\vec{\nabla}$ in the spherical coordinate basis. This term is not diagonal in that basis. Baker [1] has noticed that there is near degeneracy of the states characterized by $\omega=\lambda+[(l+1)/2]$, where $[x]$ means the largest integer less than or equal to x. At this point, for reasons of numerical expediency, he replaces the matrix elements by plus or minus the root mean square value over the nearly degenerate block. This result depends on the quantity

$$T_{l,\lambda}=-\frac{\hbar^2}{2m}\langle l,m,\lambda|\nabla_{\hat{r}}^2|l,m,\lambda\rangle. \tag{3.5}$$

By performing the sum of the matrix elements of $\hat{H}^2$ over m and then over the nearly degenerate block, Baker [1] obtains

$$\left[\frac{\hbar^2\hat{k}_B^2}{2m}\hat{\Delta}_\omega(k)\right]^2=\frac{4}{(L+1)^2}\left(\frac{\hbar^2\hat{k}^2}{2m}\right)$$
$$\times\sum_{l=0}^{L-1}\left(\frac{2l+1}{3}\right)T_{l,\omega-[(l+1)/2]}, \tag{3.6}$$

which gives the appropriate root mean square coefficient of the linear term in $\vec{k}$. This approximation is accurate to within $-2.5\%-+4.9\%$. $\hat{\Delta}$ is something like a bandwidth.

Before proceeding, it is worthwhile to describe the change in the spherical cell model to include Z electrons in one sphere. In the standard approach each electron is in its own sphere with a radius which is smaller by a factor of $Z^{1/3}$. Thus,

$$\hat{r}_b=\left(\frac{3\mathcal{A}}{4\pi\mathcal{N}_0 Z\rho}\right)^{1/3}=7.344\,995\times10^{-9}\left(\frac{\mathcal{A}}{Z\rho}\right)^{1/3}\ \text{cm}, \tag{3.7}$$

where $\mathcal{A}$ is the gram atomic weight and $\mathcal{N}_0$ is Avogadro's number. The equation for the noninteracting case is

$$\frac{\hbar^2}{2m}[\hat{k}^2-2i\vec{\hat{k}}\cdot\vec{\nabla}_{\hat{r}}-\nabla^2_{\hat{r}}]\phi_{l,\lambda}(\vec{\hat{r}})=\tilde{\mathcal{E}}_{l,\lambda}(\vec{\hat{k}})\phi_{l,\lambda}(\vec{\hat{r}}), \tag{3.8}$$

subject to the boundary conditions

$$\vec{n}\cdot\vec{\nabla}\phi_{\text{even}}(\vec{\hat{r}}_b)=0,\quad \phi_{\text{odd}}(\vec{\hat{r}}_b)=0, \tag{3.9}$$

where $\vec{n}$ is the unit normal vector to the sphere. The relevant $\vec{\hat{k}}$ are those in the first Brillouin zone, $|\vec{\hat{k}}|\leqslant\hat{k}_B$ where $\hat{k}_B=(9\pi/2)^{1/3}/\hat{r}_b$. I also define $k_B=(9\pi/2)^{1/3}/r_b$, where $r_b=\sqrt[3]{Z}\hat{r}_b$.

In the case where $\vec{\hat{k}}=\vec{0}$, the radial part of the wave functions are the spherical Bessel functions $j_l(\hat{p}_{l,\lambda}\hat{r})$ where

$$j_l(\hat{p}_{l,\lambda}\hat{r}_b)=0,\quad l\ \text{odd},$$
$$j_l'(\hat{p}_{l,\lambda}\hat{r}_b)=0,\quad l\ \text{even} \tag{3.10}$$

are the boundary conditions. The normalization condition which determines μ is

$$\begin{aligned}1&=\frac{2\Omega}{ZN}\frac{1}{(2\pi)^3}\int\frac{d\vec{\hat{k}}}{1+\exp\left(\dfrac{\hbar^2\hat{k}^2}{2mkT}-\dfrac{\mu}{kT}\right)}\\&=\frac{3}{2\pi}\int\frac{d\vec{\hat{k}}/\hat{k}_B^3}{1+\exp\left[\left(\dfrac{6\pi^2ZN}{\Omega}\right)^{2/3}\dfrac{\hbar^2}{2mkT}\dfrac{\hat{k}^2}{\hat{k}_B^2}-\dfrac{\mu}{kT}\right]}\\&\approx3\sum_{l=0}^{\infty}(2l+1)\sum_{n=0}^{\infty}\int_0^1 d\hat{\kappa}\hat{\kappa}^2\left\{\frac{1}{1+\exp[(1.5\sqrt{\pi}\zeta)^{2/3}(e_{l,n}+\hat{\kappa}^2+\hat{\kappa}\hat{\Delta}_{n+[(l+1)/2]})-\mu/kT]}\right.\\&\quad\left.+\frac{1}{1+\exp[(1.5\sqrt{\pi}\zeta)^{2/3}(e_{l,n}+\hat{\kappa}^2-\hat{\kappa}\hat{\Delta}_{n+[(l+1)/2]})-\mu/kT]}\right\},\end{aligned} \tag{3.11}$$

where I use the notation $e_{l,n}=\hat{p}_{l,n}^2/\hat{k}_B^2$ and where $3=2\times3\times\frac{1}{2}$ and the 2 is for the two electron states, the 3 normalizes the integral, and the $\frac{1}{2}$ compensates for the two $\pm\hat{\Delta}$ terms. ζ is as defined in Eq. (2.9), and $\hat{\kappa}=\hat{k}/\hat{k}_B$. In this section and beyond, N denotes the number of ions, and ZN the number of electrons.

For the pressure, remembering that $p\Omega$ is just $\frac{2}{3}$ of the energy I get

$$\begin{aligned}\frac{p\Omega}{ZNkT}&\approx2(1.5\sqrt{\pi}\zeta)^{2/3}\sum_{l=0}^{\infty}(2l+1)\sum_{n=0}^{\infty}\int_0^1 d\hat{\kappa}\hat{\kappa}^2\left\{\frac{e_{l,n}+\hat{\kappa}^2+\hat{\kappa}\hat{\Delta}_{n+[(l+1)/2]}(k_B)}{1+\exp[(1.5\sqrt{\pi}\zeta)^{2/3}(e_{l,n}+\hat{\kappa}^2+\hat{\kappa}\hat{\Delta}_{n+[(l+1)/2]})-\mu/kT]}\right.\\&\quad\left.+\frac{e_{l,n}+\hat{\kappa}^2-\hat{\kappa}\hat{\Delta}_{n+[(l+1)/2]}(k_B)}{1+\exp[(1.5\sqrt{\pi}\zeta)^{2/3}(e_{l,n}+\hat{\kappa}^2-\hat{\kappa}\hat{\Delta}_{n+[(l+1)/2]})-\mu/kT]}\right\}.\end{aligned} \tag{3.12}$$

Let us expand the volume to encompass Z electrons instead of 1. Then Eq. (3.9) becomes

$$\vec{n}\cdot\vec{\nabla}\phi_{\text{even}}(Z^{1/3}\vec{\hat{r}}_b)=0,\quad \phi_{\text{odd}}(Z^{1/3}\vec{\hat{r}}_b)=0. \tag{3.13}$$

The electron-ion interaction is given by Eq. (3.1) in a sphere of radius r_b. For the independent electron case I need to transform this equation to the smaller sized sphere $|\vec{r}|\leqslant\hat{r}_b$ appropriate to the single independent electron. The change of variables is $\hat{r}=r/Z^{1/3}$ and $\hat{k}=Z^{1/3}k$, which gives

$$Z^{2/3}\left\{\frac{\hbar^2}{2m^*}[k^2-2i\vec{k}\cdot\vec{\nabla}-\nabla^2]-\frac{e^2Z^{-1/3}v(r_b,T,r/r_b)}{r}\right.$$
$$\left.-\frac{e^2Z^{-1/3}}{2r_b}\left(\frac{r}{r_b}\right)^2F\left(\frac{y^2}{Z}\right)\right\}\phi_{l,\lambda}(\vec{r})$$
$$=\tilde{\mathcal{E}}_{l,\lambda}(\vec{k})\phi_{l,\lambda}(\vec{r}). \tag{3.14}$$

The overall factor of $Z^{2/3}$ on the left hand side converts the divisor in $e_{l,n}$ from $\hat{k}_B^2$ to k_B^2. This result is in accord with the well known result that, for the ideal Fermi gas, μ is a function of ζ alone.

For the sake of clarity, I summarize. Eq. (3.1) becomes

$$\left\{\frac{\hbar^2}{2m^*}[k^2-2i\vec{k}\cdot\vec{\nabla}-\nabla^2]-\frac{e^2Z^{-1/3}v(r_b,T,r/r_b)}{r}\right.$$
$$\left.-\frac{e^2Z^{-1/3}}{2r_b}\left(\frac{r}{r_b}\right)^2F\left(\frac{y^2}{Z}\right)\right\}\phi_{l,\lambda}(\vec{r})$$
$$=\mathcal{E}_{l,\lambda}(\vec{k})\phi_{l,\lambda}(\vec{r}), \tag{3.15}$$

with the boundary conditions given by Eq. (3.9). In the spherical cell approximation the normalization condition which determines μ is

$$1=3\sum_{l=0}^{\infty}(2l+1)\sum_{n=0}^{\infty}\int_0^1 d\hat{\kappa}\hat{\kappa}^2\left\{\frac{1}{1+\exp\left\{(1.5\sqrt{\pi}\zeta)^{2/3}\left[e_{l,n}+\frac{1}{2}\left(1+\frac{m^*}{m}\right)(\hat{\kappa}^2+\hat{\kappa}\hat{\Delta}_{n+[(l+1)/2]})\right]-\mu/kT\right\}}\right.$$
$$\left.+\frac{1}{1+\exp\left\{(1.5\sqrt{\pi}\zeta)^{2/3}\left[e_{l,n}+\frac{1}{2}\left(1+\frac{m^*}{m}\right)(\hat{\kappa}^2-\hat{\kappa}\hat{\Delta}_{n+[(l+1)/2]})\right]-\mu/kT\right\}}\right\}, \tag{3.16}$$

where now the dimensionless form of the eigenvalue is

$$e_{l,n}=\frac{2m\epsilon_{l,n}(\vec{0})}{\hbar^2k_B^2}. \tag{3.17}$$

For the corresponding ϵ,

$$\epsilon_{l,\lambda}(\vec{k})=\frac{1}{2}\left(1+\frac{m^*}{m}\right)\left[\mathcal{E}_{l,\lambda}(\vec{k})-\frac{1}{2}\langle\phi_{l,\lambda}(\vec{r})|\left(\frac{Z^{2/3}e^2}{r}-\frac{e^2v(r_b,T,r/r_b)Z^{-1/3}}{r}\right)|\phi_{l,\lambda}(\vec{r})\rangle\right]$$
$$-\frac{1}{2}\left(1-\frac{m*}{m}\right)\langle\phi_{l,\lambda}(\vec{r})|\frac{v(r_b,T,r/r_b)e^2Z^{-1/3}}{r}|\phi_{l,\lambda}(\vec{r})\rangle+\frac{m^*e^2Z^{-1/3}}{4mr_b}F\left(\frac{y^2}{Z}\right)\langle\phi_{l,\lambda}(\vec{r})|\frac{r^2}{r_b^2}|\phi_{l,\lambda}(\vec{r})\rangle+\Delta\epsilon. \tag{3.18}$$

where the state independent part is

$$\Delta\epsilon_{||}=Z^{-1/3}\left\{\frac{3e^2}{10r_b}g(y^2)+\frac{3Ze^2}{5r_b}F(y^2Z)\right.$$
$$\left.+\frac{e^2}{r_b}F\left(\frac{y^2}{Z}\right)\left[\frac{3}{4}-\left(\frac{3Z}{\pi\zeta}\right)^{1/3}f_{1/2}(z(\zeta))\right]\right\},$$

$$\Delta\epsilon_{\text{anti-}||}=Z^{-1/3}\left\{\frac{3e^2}{10r_b}g(y^2)+\frac{3Ze^2}{5r_b}F(y^2Z)+\frac{3e^2}{4r_b}F\left(\frac{y^2}{Z}\right)\right\}. \tag{3.19}$$

Again, for the antiparallel case $m^*/m=1$ and I drop the $f_{1/2}$ term.

It is not trivial to organize the spherical cellular model equations so that they can be implemented with currently available computers. Indeed, there are rather serious computational challenges in the production of numerical results for this model. Not surprisingly, the problems become more significant as the value of Z increases. Unless the work is properly organized, there is the issue of having to store more data in high speed memory than is available in even very large modern computers. If one stores the data on the hard drives, then the computation slows down by an impractically large amount. The equations of Appendix A (together with those in the body of the paper) implicitly lay out how I have solved the computational organization in order to get the results reported. This method does solve the storage problem, but even so, hundreds of hours of work station time were required.

When I evaluate these equations numerically, there is the issue of the number of values of l required. I impose two conditions. First that the minimum of the potential for the largest value of l lies on the surface, or outside the cell. Second that the potential value at the surface for that value of l be at least $15kT$ which gives a factor of about 10^{-6} for those states. These conditions imply that

$$L \geqslant \frac{1}{2}[\sqrt{1+7.082731x_0(Z^{2/3}+15Z/y^2)}-1]+10, \tag{3.20}$$

where the 10 is just added for safety's sake.

A sufficient number of mesh spaces for the radial coordinate was determined by Baker [1] for the case $Z=1$ to be the maximum of $16x_0$ and $2x_0\sqrt{T}$ where T is in eV, and

$$x_0=\left(\frac{128}{9\pi^2}\right)^{1/3}\frac{me^2r_b}{\hbar^2}=1.567\,778\left(\frac{\mathcal{A}}{\rho}\right)^{1/3},$$

$$\frac{2r_bme^2}{\hbar^2}=1.770\,682\,75x_0, \tag{3.21}$$

with ρ in g/cm^3. On account of the factor of $Z^{2/3}$, and the known dependence of the eigenfunctions, I take the mesh spacing to be the maximum of $16Z^{2/3}x_0$ and $2x_0\sqrt{T}$. The number of mesh spaces in the k integration remains unchanged at $16(1.5\sqrt{\pi}\zeta)^{1/3}$, as the Z dependence is incorporated in the definition of ζ.

By Eqs. (2.4) and (2.6) in order to compute the pressure and the internal energy, I need in addition to the ϵ's, their derivatives with respect to r_b and T. First following Appendix A of Baker [1], I need

$$r_b\frac{\partial\mathcal{E}}{\partial r_b}=-\left(2+\frac{\partial\ln m^*}{\partial\ln r_b}\right)\mathcal{E}+Z^{-1/3}r_b^3\int d\vec{\rho}\,\phi^*(r_b,\vec{\rho})\left\{-\frac{e^2r_bv'(r_b,T,\rho)}{r}\right.$$
$$\left.-\left(1+\frac{\partial\ln m^*}{\partial\ln r_b}\right)\left[\frac{e^2v(r_b,T,r/r_b)}{r}+\frac{e^2}{2r_b}\left(\frac{r}{r_b}\right)^2F\left(\frac{y^2}{Z}\right)\right]+\frac{e^2}{2r_b}\rho^2\frac{y^2}{Z}F'\left(\frac{y^2}{Z}\right)\right\}\phi(r_b,\vec{\rho}), \tag{3.22}$$

where $\vec{\rho}\equiv\vec{r}/r_b$. Using this result, I can write

$$r_b\frac{\partial}{\partial r_b}\epsilon_{l,\lambda}(\vec{k})=-\frac{1}{2}\left(1+\frac{m^*}{m}\right)\left(\left(2+\frac{\partial\ln m^*}{\partial\ln r_b}\right)\left[\mathcal{E}_{l,\lambda}(\vec{0})+\frac{\hbar^2k^2}{2m^*}\pm\frac{\hbar^2k_B^2}{2m^*}\Delta_{l,\lambda}(k)\right]-Z^{-1/3}\langle\phi_{l,\lambda}(\vec{r})|\left\{\frac{e^2r^2}{2Zr_b^3}y^2F'\left(\frac{y^2}{Z}\right)\right.\right.$$
$$\left.\left.-\left(1+\frac{\partial\ln m^*}{\partial\ln r_b}\right)\left[\frac{e^2v(r_b,T,r/r_b)}{r}+\frac{e^2r^2}{2r_b^3}F\left(\frac{y^2}{Z}\right)\right]\right\}|\phi_{l,\lambda}(\vec{r})\rangle\right)+\frac{1}{2m}\frac{\partial m^*}{\partial\ln r_b}$$
$$\times\left[\mathcal{E}_{l,\lambda}(\vec{0})+\frac{\hbar^2k^2}{2m^*}\pm\frac{\hbar^2k_B^2}{2m^*}\Delta_{l,\lambda}(k)-\frac{1}{2}\langle\phi_{l,\lambda}(\vec{r})|\left(\frac{Z^{2/3}e^2}{r}-\frac{e^2v(r_b,T,r/r_b)Z^{-1/3}}{r}\right)|\phi_{l,\lambda}(\vec{r})\rangle\right]$$
$$+r_b\frac{\partial}{\partial r_b}\Delta\epsilon_{||}-\frac{1}{2}Z^{-1/3}\left(1+\frac{m^*}{m}\right)\langle\phi_{l,\lambda}(\vec{r})|\frac{e^2r_bv'(r_b,T,\rho)}{r}|\phi_{l,\lambda}(\vec{r})\rangle+Z^{-1/3}r_b\frac{\partial}{\partial r_b}\langle\phi_{l,\lambda}(\vec{r})|$$
$$\times\left[-\frac{e^2}{2r_b}\left(1-\frac{m^*}{m}\right)\frac{v(r_b,T,r/r_b)}{r/r_b}+\frac{m^*e^2r^2}{4mr_b^3}F\left(\frac{y^2}{Z}\right)\right]|\phi_{l,\lambda}(\vec{r})\rangle+\frac{e^2}{4Z^{1/3}r_b}\left(1+\frac{m^*}{m}\right)\langle\phi_{l,\lambda}(\vec{r})|$$
$$\times\left(\frac{Z}{r/r_b}-\frac{v(r_b,T,r/r_b)}{r/r_b}\right)|\phi_{l,\lambda}(\vec{r})\rangle-\frac{e^2}{4Z^{1/3}r_b}\left(1+\frac{m^*}{m}\right)r_b\frac{\partial}{\partial r_b}\langle\phi_{l,\lambda}(\vec{r})|\left(\frac{Z}{r/r_b}-\frac{v(r_b,T,r/r_b)}{r/r_b}\right)|\phi_{l,\lambda}(\vec{r})\rangle \tag{3.23}$$

for the case of parallel spins. For the case of antiparallel spins, I write

$$r_b\frac{\partial}{\partial r_b}\epsilon_{l,\lambda}(\vec{k})=-2\left[\mathcal{E}_{l,\lambda}(\vec{0})+\frac{\hbar^2k^2}{2m^*}\pm\frac{\hbar^2k_B^2}{2m^*}\Delta_{l,\lambda}(k)\right]+Z^{-1/3}\langle\phi_{l,\lambda}(\vec{r})|\left[\frac{e^2r^2}{2Zr_b^3}y^2F'\left(\frac{y^2}{Z}\right)-\frac{e^2v(r_b,T,r/r_b)}{r}\right.$$
$$\left.-\frac{e^2r^2}{2r_b^3}F\left(\frac{y^2}{Z}\right)\right]|\phi_{l,\lambda}(\vec{r})\rangle-Z^{-1/3}\langle\phi_{l,\lambda}(\vec{r})|\frac{e^2r_bv'(r_b,T,\rho)}{r}|\phi_{l,\lambda}(\vec{r})\rangle$$
$$+Z^{-1/3}r_b\frac{\partial}{\partial r_b}\langle\phi_{l,\lambda}(\vec{r})|\frac{e^2r^2}{4r_b^3}F\left(\frac{y^2}{Z}\right)|\phi_{l,\lambda}(\vec{r})\rangle+\frac{e^2}{2Z^{1/3}r_b}\langle\phi_{l,\lambda}(\vec{r})|\left(\frac{Z}{r/r_b}-\frac{v(r_b,T,r/r_b)}{r/r_b}\right)|\phi_{l,\lambda}(\vec{r})\rangle$$
$$+r_b\frac{\partial}{\partial r_r}\Delta\epsilon_{\text{anti-}||}-\frac{e^2}{2Z^{1/3}r_b}r_b\frac{\partial}{\partial r_b}\langle\phi_{l,\lambda}(\vec{r})|\left(\frac{Z}{r/r_b}-\frac{v(r_b,T,r/r_b)}{r/r_b}\right)|\phi_{l,\lambda}(\vec{r})\rangle, \tag{3.24}$$

where

$$r_b\frac{\partial}{\partial r_r}\Delta\epsilon_{||}=-\frac{e^2}{r_b}Z^{-1/3}\left\{\frac{3}{10}g(y^2)+\frac{3}{10}y^2g'(y^2)+\frac{3}{5}Z[F(y^2Z)+y^2ZF'(y^2Z)]+\frac{3}{4}\left[F\left(\frac{y^2}{Z}\right)+\frac{y^2}{Z}F'\left(\frac{y^2}{Z}\right)\right]\right.$$
$$\left.-\left(\frac{3Z}{\pi\zeta}\right)^{1/3}\left[f_{1/2}(z(\zeta))\frac{y^2}{Z}F'\left(\frac{y^2}{Z}\right)+3\zeta f'_{1/2}(z(\zeta))F\left(\frac{y^2}{Z}\right)\right]\right\},$$

$$r_b\frac{\partial}{\partial r_r}\Delta\epsilon_{\text{anti-}||}=-\frac{e^2}{r_b}Z^{-1/3}\left\{\frac{3}{10}g(y^2)+\frac{3}{10}y^2g'(y^2)+\frac{3}{5}Z[F(y^2Z)+y^2ZF'(y^2Z)]+\frac{3}{4}\left[F\left(\frac{y^2}{Z}\right)+\frac{y^2}{Z}F'\left(\frac{y^2}{Z}\right)\right]\right\}. \tag{3.25}$$

Again, for the antiparallel case $m^*/m=1$ and I have dropped the $f_{1/2}$ terms. In the above equations, F', $f'_{1/2}$, and g' are the derivatives with respect to the arguments. v' is the derivative with respect to r_b. In the following equations, $\dot{v}$ is the derivative with respect to T.

The details of the calculation of the above quantities and also those for the temperature derivatives are treated in Appendix A.

Next I need the derivative of Eq. (3.18) with respect to T. The first ingredient that I need is

$$T\frac{\partial\mathcal{E}}{\partial T}=-\frac{T}{m^*}\frac{\partial m^*}{\partial T}\left\{\mathcal{E}+Z^{-1/3}\int d\vec{r}\phi^*(\vec{r})\left[\frac{e^2v(r_b,T,r/r_b)}{r}+\frac{e^2r^2}{2r_b^3}F\left(\frac{y^2}{Z}\right)\right]\phi(\vec{r})\right\}$$
$$+Z^{-1/3}\int d\vec{r}\phi^*(\vec{r})\left[e^2F'\left(\frac{y^2}{Z}\right)\frac{y^2}{2r_bZ}\left(\frac{r}{r_b}\right)^2-\frac{e^2T\dot{v}(r_b,T,r/r_b)}{r}\right]\phi(\vec{r}). \tag{3.26}$$

Hence I have

$$T\frac{\partial}{\partial T}\epsilon_{l,\lambda}(\vec{k})=-\frac{\partial\ln m^*}{\partial\ln T}\left[\frac{1}{2}\mathcal{E}_{l,\lambda}(\vec{k})+\frac{1}{2}Z^{-1/3}\left(1+\frac{m^*}{m}\right)\langle\phi_{l,\lambda}(\vec{r})|\frac{e^2v(r_b,T,r/r_b)}{r}+\frac{e^2r^2}{2r_b^3}F\left(\frac{y^2}{Z}\right)\right.$$
$$\left.+\frac{m^*}{4m}\left(\frac{Z^{2/3}e^2}{r}-\frac{e^2v(r_b,T,r/r_b)}{r}\right)|\phi_{l,\lambda}(\vec{r})\rangle\right]+\frac{1}{2}Z^{-1/3}\left(1+\frac{m^*}{m}\right)\langle\phi_{l,\lambda}|\frac{e^2r^2}{2r_b^3}F'\left(\frac{y^2}{Z}\right)\frac{y^2}{Z}$$
$$-\frac{e^2}{r}T\dot{v}(r_b,T,r/r_b)|\phi_{l,\lambda}(\vec{r})\rangle+Z^{-1/3}T\frac{\partial}{\partial T}\langle\phi_{l,\lambda}(\vec{r})|\left\{-\frac{1}{2}\left(1-\frac{m^*}{m}\right)\frac{e^2v(r_b,T,r/r_b)}{r}\right.$$
$$\left.+\frac{m^*}{4m}\frac{e^2r^2}{r_b^3}F\left(\frac{y^2}{Z}\right)\right\}|\phi_{l,\lambda}(\vec{r})\rangle-\frac{e^2}{4Z^{1/3}r_b}\left(1+\frac{m^*}{m}\right)T\frac{\partial}{\partial T}\langle\phi_{l,\lambda}(\vec{r})|\frac{Z}{r/r_b}-\frac{v(r_b,T,r/r_b)}{r/r_b}|\phi_{l,\lambda}(\vec{r})\rangle+T\frac{\partial}{\partial T}\Delta\epsilon_{||}, \tag{3.27}$$

and for the antiparallel case,

$$T\frac{\partial}{\partial T}\epsilon_{l,\lambda}(\vec{k}) = Z^{-1/3}\langle\phi_{l,\lambda}|\frac{e^2r^2}{2r_b^3}F'\left(\frac{y^2}{Z}\right)\frac{y^2}{Z} - \frac{e^2}{r}T\dot{v}(r_b,T,r/r_b)|\phi_{l,\lambda}(\vec{r})\rangle + Z^{-1/3}T\frac{\partial}{\partial T}\langle\phi_{l,\lambda}(\vec{r})|\frac{m^*}{4m}\frac{e^2r^2}{r_b^3}F\left(\frac{y^2}{Z}\right)|\phi_{l,\lambda}(\vec{r})\rangle - \frac{e^2}{2Z^{1/3}r_b}T\frac{\partial}{\partial T}\langle\phi_{l,\lambda}(\vec{r})|\frac{Z}{r/r_b} - \frac{v(r_b,T,r/r_b)}{r/r_b}|\phi_{l,\lambda}(\vec{r})\rangle + T\frac{\partial}{\partial T}\Delta\epsilon_{\text{anti-}||}, \tag{3.28}$$

where

$$T\frac{\partial}{\partial T}\Delta\epsilon_{||} = -\frac{3}{10}Z^{-1/3}g'(y^2)y^2 - \frac{3Z^{5/3}e^2}{5r_b}y^2F'(y^2Z) - \frac{e^2}{r_b}Z^{-1/3}F'\left(\frac{y^2}{Z}\right)\frac{y^2}{Z}\left[\frac{3}{4} - \left(\frac{3Z}{\pi\zeta}\right)^{1/3}f_{1/2}(\zeta)\right] + \frac{e^2}{r_b}Z^{-1/3}F\left(\frac{y^2}{Z}\right)\left[-\left(\frac{3Z}{\pi\zeta}\right)^{1/3}f_{1/2}(\zeta) + \frac{3}{2}\left(\frac{3Z}{\pi\zeta}\right)^{1/3}\zeta f'_{1/2}(\zeta)\right],$$

$$T\frac{\partial}{\partial T}\Delta\epsilon_{\text{anti-}||} = -\frac{3}{10}Z^{-1/3}g'(y^2)y^2 - \frac{3Z^{5/3}e^2}{5r_b}y^2F'(y^2Z) - \frac{3e^2}{4r_b}Z^{-1/3}F'\left(\frac{y^2}{Z}\right)\frac{y^2}{Z}. \tag{3.29}$$

Next I consider the problem of the self-consistent potential. To this end, I use Poisson's equation

$$\nabla^2V(\vec{r}) = e^2\varrho. \tag{3.30}$$

The potential V is obtained from the charge density ϱ by the solution of this equation. To be consistent with Eq. (3.1), I take the convention that the electron charge density is positive instead of the usual convention that it is negative. The solution for a heterogeneous sphere of radius r_b with spherical symmetry is [15]

$$V(r) = -e^2\frac{1}{r}\int_0^r\varrho(\alpha)\alpha^2d\alpha - e^2\int_r^{r_b}\varrho(\alpha)\alpha d\alpha \tag{3.31}$$

which is

$$rV(r)/e^2 = -\int_0^{r_b}\varrho(\alpha)\alpha^2d\alpha + \int_r^{r_b}\varrho(\alpha)\alpha^2d\alpha - r\int_r^{r_b}\varrho(\alpha)\alpha d\alpha. \tag{3.32}$$

Now, the first term on the right hand side is just $-Z$. To complete the computation of the potential, I need to add Z to take account of the central ionic charge. Thus,

$$rV(r)/e^2 = \int_r^{r_b}\left(1-\frac{r}{\alpha}\right)\varrho(\alpha)\alpha^2d\alpha. \tag{3.33}$$

Done properly, to obtain the self-consistent potential $-e^2v(r_r,T,r/r_b)/r$, the electron density which corresponds to the state being computed in the solution of Eq. (3.1) should be subtracted from the total charge density. However I will instead simplify the process by subtracting the $1/Z$ fraction of the density. There will of course then be an uncompensated unit ionic charge contribution to the potential. Thus I obtain

$$v(r_b,T,r/r_b) = 1 + \left(\frac{Z-1}{Z}\right)r_b\int_{(r/r_b)}^1\left(1-\frac{r}{\beta r_b}\right)\times\mathcal{D}(r_b,T,\beta)d\beta. \tag{3.34}$$

For the case of a uniform density $\mathcal{D}(r_b,T,r/r_b) = 3Zr^2/r_b^3$, and $v(r_b,T,r/r_b) = Z + \frac{1}{2}(Z-1)[(r/r_b)^3 - 3(r/r_b)]$. I use this value as an initial guess to start the self-consistent iteration process. The potential of Eq. (3.34) corresponds to the complete ionic charge at the origin, and just the hydrogen potential at the surface of (and outside) the sphere. When $Z=1$, this potential reduces correctly to that for hydrogen. The cellular model charge density is

$$\mathcal{D}(r_b,T,r/r_b) = \sum_{l,\lambda}\frac{(2l+1)\phi^*_{l,\lambda}(r)\phi_{l,\lambda}(r)r^2}{\exp[(\epsilon_{l,\lambda}-\mu)/kT]+1}. \tag{3.35}$$

To complete the calculations, I will also need the weighted charge density

$$\mathcal{D}^*(r_b,T,r/r_b) = \sum_{l,\lambda}\frac{m^*(\lambda)(2l+1)\phi^*_{l,\lambda}(r)\phi_{l,\lambda}(r)r^2}{m\{\exp[(\epsilon_{l,\lambda}-\mu)/kT]+1\}}, \tag{3.36}$$

where in states λ with antiparallel spins, $m^*(\lambda)$ is taken to be m.

I have programmed these equations for a computer to produce the pressure, the internal energy, and the "physically reasonable" energy (5.2) as functions of the temperature and the density. I report the results of computations made for this model in the following two sections.

IV. LIMITING CASES

The equation of state tends to that of the ideal Fermi gas (plus the Maxwell-Boltzmann behavior of the ions) in a number of special limiting cases. The most obvious case is when $y \to 0$. Here the structure of the many-body terms, as discussed in the preceding section, is such that the ideal-gas limit and the leading order terms $[O(y^2)]$ are correctly given. Note that the spherical approximation for the cells causes a few per cent fluctuation about the correct ideal-gas value. For the pure ideal-gas case, this fluctuation is not more than 5%.

The next limiting case of interest is the behavior of a very dense system. It is well known that in this limit the kinetic energy per electron [see Eq. (2.9)] is proportional to $\rho^{2/3}$, while potential energy is only proportional to $\rho^{1/3}$. Thus I expect the kinetic energy to dominate and the system to tend to ideal-gas behavior in this limit. The system will be approximately independent of temperature for the temperature below the Fermi temperature.

When the temperature is small compared to μ, defined by Eq. (2.2), and the system is dense, the level density at the Fermi surface is approximately that of an ideal gas. Thus I may follow the standard derivation (see, for example, Ref. [12]) to find the temperature variation to leading order. The result is

$$p = p(T=0,\Omega)\left[1+\frac{5\pi^2}{12}\left(\frac{T}{\mu}\right)^2+\cdots\right],$$

$$U = U(T=0,\Omega)\left[1+\frac{5\pi^2}{12}\left(\frac{T}{\mu}\right)^2+\cdots\right]. \qquad (4.1)$$

One expects, as the ideal-gas behavior only depends on ζ, that $\mu \propto \rho^{2/3}$ in the high-density limit. This behavior is illustrated for lithium in Fig. 1. Figure 2 shows the behavior of the cellular model pressure with Coulomb interactions. The dominant physical behavior of temperature independence for high density and modest temperature is well illustrated in Fig. 2. Here the electron pressure divided by the ideal-gas pressure shows rather good data collapse for the case of lithium. It is of interest to compare the high-density behavior (in the one-phase region) with that of the Thomas-Fermi model evaluated at zero temperature [14]. I show such results for cesium at $T=1$ eV in Fig. 3. The spherical cellular model pressure decreases relative to the Thomas-Fermi pressure noticeably in this region as the density decreases. We also see in this figure that the Thomas-Fermi pressure is less than the ideal-gas pressure. I have investigated numerically the departure from the limiting curve seen in Fig. 2, and I find that it is rather different from that predicted by Eq. (4.1). I illustrate these results in Fig. 4 for the case of potassium. I have determined numerically that in the limit of high densities, the deviation

$$\Delta = 1 - \frac{p_{\text{electron}}(\rho,T)p_{\text{ideal}}(\rho,T=0)}{p_{\text{ideal}}(\rho,T)p_{\text{electron}}(\rho,T=0)} \qquad (4.2)$$

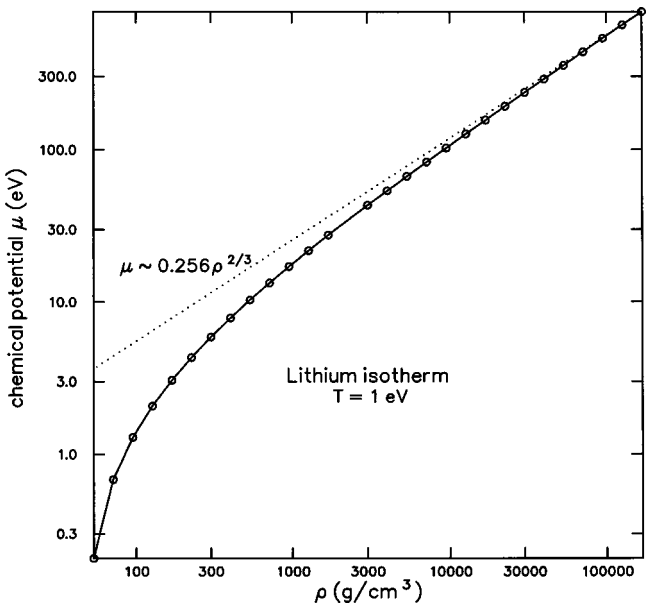

FIG. 1. The chemical potential μ of the spherical cellular model for lithium ($Z=3$) vs the density. These results are for the 1-eV isotherm. The dotted line shows the asymptote proportional to $\rho^{2/3}$.

from the zero-temperature limit is $\Delta \asymp \hat{\mathrm{d}}(Z)/Ty^{12}$. The symbol $\asymp$ means asymptotic. Put otherwise the deviation is $\Delta \asymp \mathrm{d}(Z)/y^8\zeta^{2/3}$. I have estimated that $\mathrm{d}(3) \approx 2.1\times 10^5$, $\mathrm{d}(19) \approx 3.4\times 10^7$, $\mathrm{d}(55) \approx 5.7\times 10^9$.

In the low-density limit, Baker and Johnson [14] found from the perturbation expansion that

$$\frac{p_{\text{electron}}(\Omega,T)}{p_{\text{ideal}}(\Omega,T)} \asymp 1 - \frac{1}{\sqrt{3}}\frac{(Z+1)^{3/2}}{2Z}y^3+\cdots. \qquad (4.3)$$

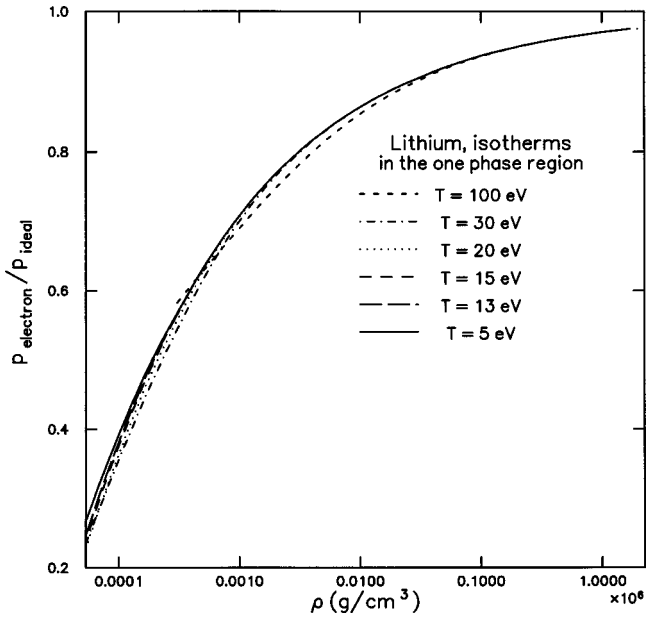

FIG. 2. The ratio of the electron pressure to the ideal-gas pressure for several lithium ($Z=3$) isotherms at high density.

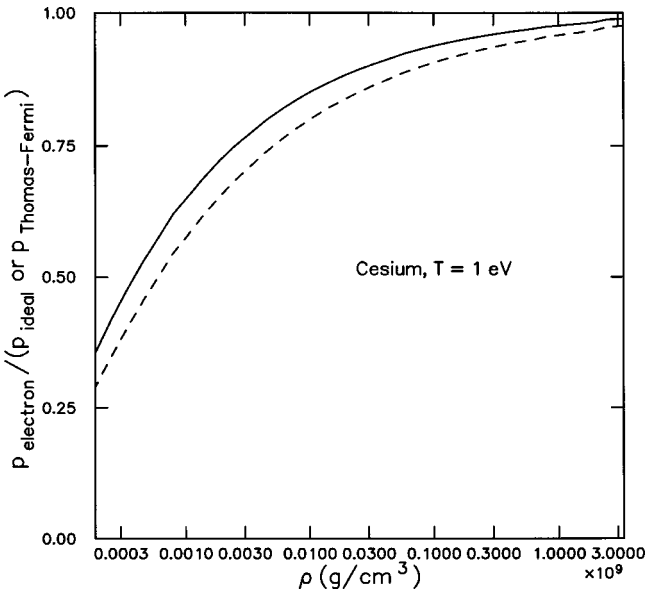

FIG. 3. The dashed line is the ratio of the electron pressure to the ideal Fermi gas pressure and the solid line is the ratio of the electron gas pressure to the $T=0$ Thomas-Fermi theory pressure. The electron gas pressure is that computed from the spherical cellular model of cesium ($Z=55$) at $T=1$ eV.

When one remembers that p_{ideal} is the ideal (uncharged) electron gas pressure, then it is easy to see that Eq. (4.3) displays just the classical Debye-Hückel correction term [16]. I do not see this simple behavior for the low-density limit. The reason is either that the higher-order terms in y are very important or that the approximations involved in this model do not adequately reproduce this limiting behavior. Equation (4.3) does however, generally speaking, indicate where the spherical cellular model results begin to deviate from the ideal gas. I have illustrated a typical case (potassium) in Fig. 5.

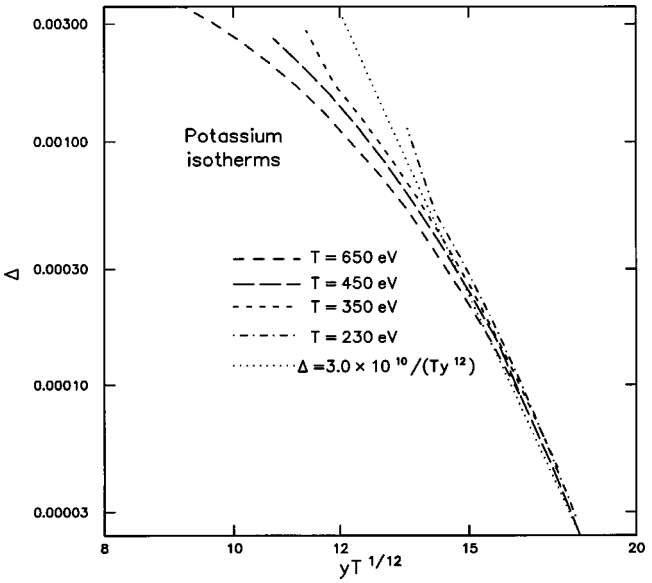

FIG. 4. The deviation $\Delta=1-[p_{\text{electron}}(\rho,T)p_{\text{ideal}}(\rho,1\text{ eV})]/[p_{\text{electron}}(\rho,1\text{ eV})p_{\text{ideal}}(\rho,T)]$ from the zero-temperature limit [Eq. (4.2)] approximated here by the 1-eV curve) of the pressure for several potassium ($Z=19$) isotherms at high density.

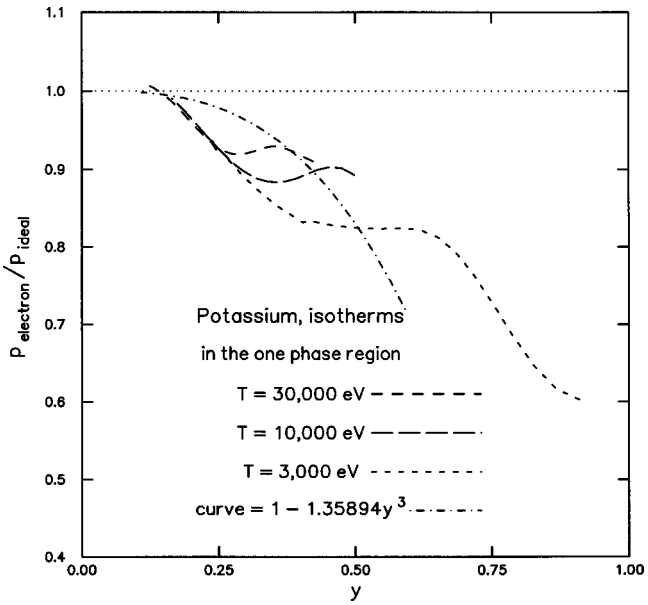

FIG. 5. The ratio of the electron pressure to the ideal-gas pressure for several potassium ($Z=19$) isotherms at low density. The dot-dashed curve is the result of Eq. (4.3).

V. NUMERICAL RESULTS

In the preceding section I was concerned with the high- and low-density limits. In this section I will look at the intermediate cases. Since the region of principal interest is the one-phase region, it is important to investigate any possible critical points and their pendant phase boundaries. The critical points described in this section are basically in the plasma regime and are not relevant to the ordinary, familiar, gas-liquid transitions. They probably represent localization-delocalization transitions as the electrons from various shells are ionized. As an example, the gas-liquid critical temperature of sodium was found experimentally [17] to be about 0.222 eV which is about 1000 times smaller than what is found here. The previous results [1] for hydrogen have compared well with a number of other calculations as reported in Ref. [18]. The author is unaware of theoretical estimates of the critical-point parameters for ''plasma phase transitions'' for elements with higher Z.

I have computed, using the criteria

$$\left.\frac{\partial p}{\partial \Omega}\right|_T = \left.\frac{\partial^2 p}{\partial \Omega^2}\right|_T = 0, \tag{5.1}$$

approximate values for the critical points which are implied. In order to locate these critical points, I have computed a number of isotherms and plotted the pressure against the volume. An illustration is shown in Fig. 6 for nitrogen. I have used the Maxwell equal area construction to locate approximately the phase boundaries. To locate the critical point I interpolate between nearby isotherms. The interpolating function is linear in the temperature and a cubic in the vol-

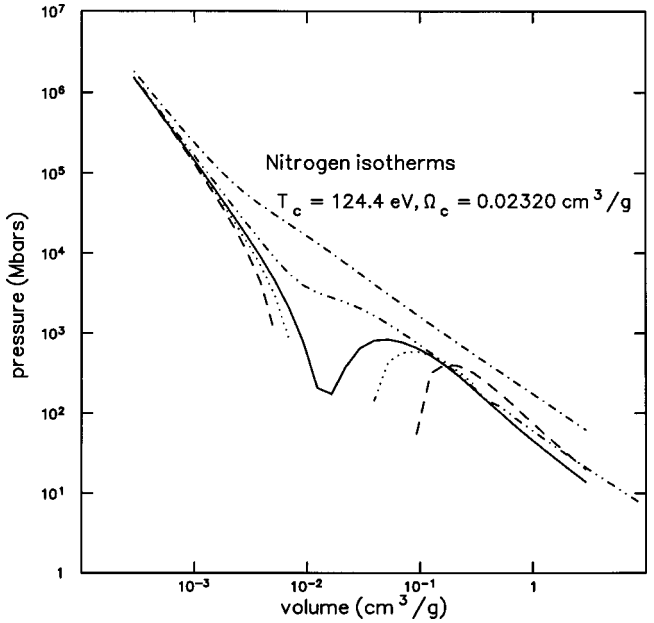

FIG. 6. Some isotherms for nitrogen ($Z=7$). The breaks in the curves occur when the computed pressure is negative. This feature is interpreted as the low part of a ''van der Waals loop'' which is to be replaced by a flat line determined by the Maxwell construction.

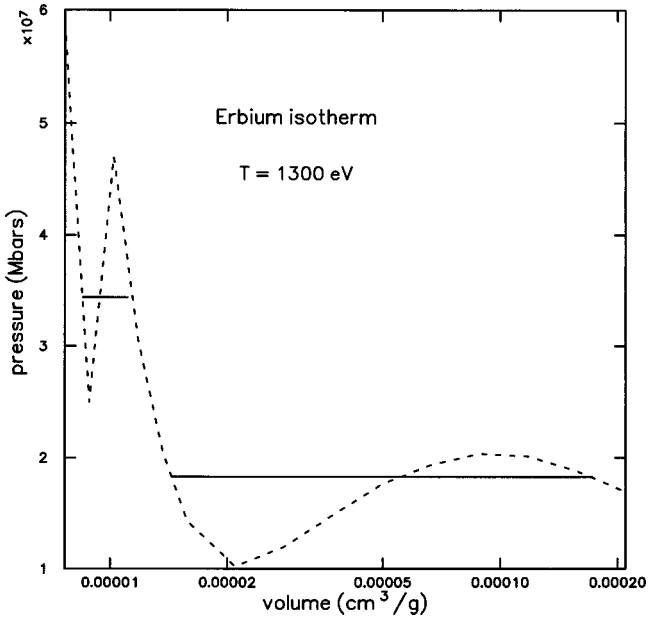

FIG. 7. An isotherm for erbium ($Z=68$). This case illustrates the possibility of having two two-phase regions. The $T=1300$ eV isotherm is illustrated by the dashed curve. The Maxwell construction which maintains monotonicity of the pressure as a function of the volume for a fixed temperature is shown by the solid horizontal lines. The reason that the equal area feature of the Maxwell construction is not visually apparent is that the volume is plotted on a log scale so that the low volume two-phase region would be clearly seen. The discontinuities in slope result from the joining of the computed values by straight lines.

ume. The reason for the use of a cubic is that on the critical isotherm $p-p_c \propto (\Omega-\Omega_c)^3$ in the neighborhood of the critical point T_c, Ω_c.

It happens for the elements with higher values of Z that (at least) two separate critical points can occur. I illustrate this case for erbium in Fig. 7. Since the imputed two-phase regions encompass the highly complex phase diagrams of solid state physics, I interpret these obtained critical properties as a possible indication of the general location of the limits of applicability of this model. However, if there are in fact plasma phase-transitions, then the actual region of validity may not be limited by these computed critical phenomena. I report results for $Z=1$, 3, 7, 11, 19, 28, 37, 46, 55, and 68. That is, for hydrogen, lithium, nitrogen, sodium, potassium, nickel, rubidium, palladium, cesium, and erbium.

It is of some interest to see a typical, radial, electron density. In Fig. 8 I have plotted the results of the spherical cellular model for erbium over a range of densities. It will be observed that at the lowest density on the surface of the sphere the density does not vanish. This feature is due to the boundary conditions which, for even parity states, impose the condition that the radial derivative vanishes and not the wave function. It is well known [21] that this condition, which is similar to the so called ''metallic bond,'' may lead to a lower energy state than that for an isolated atom. As the density increases, the change in the radial, electron density profile reflects, as one would expect, the pressure ionization of the atoms.

In Figs. 9–11, I plot the critical values of the electron pressure, electron density, and the temperature. The power laws plotted in these, and in subsequent figures, are only intended to indicate general trends as there are manifestly significant deviations from them. A second critical point has

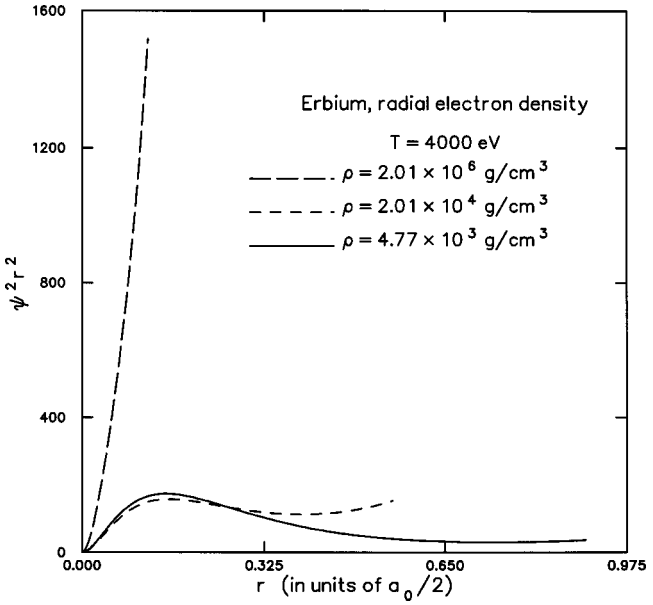

FIG. 8. The radial, electron density times r^2 computed for the spherical model for erbium, $Z=68$, at a temperature of 4000 eV. For high compression, the weighted sum of ψ^2 is nearly constant, whereas for lower densities, a concentration is seen. a_0 is the Bohr radius.

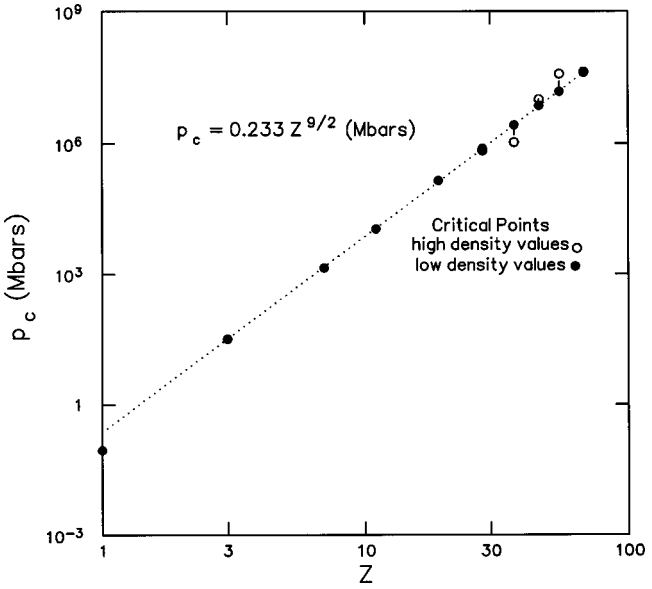

FIG. 9. The values of the critical-point electron pressure p_c vs the ion charge Z for a few selected elements. The dotted line shows the power law. The values for the two distinct critical points found for each element are connected by dashed lines.

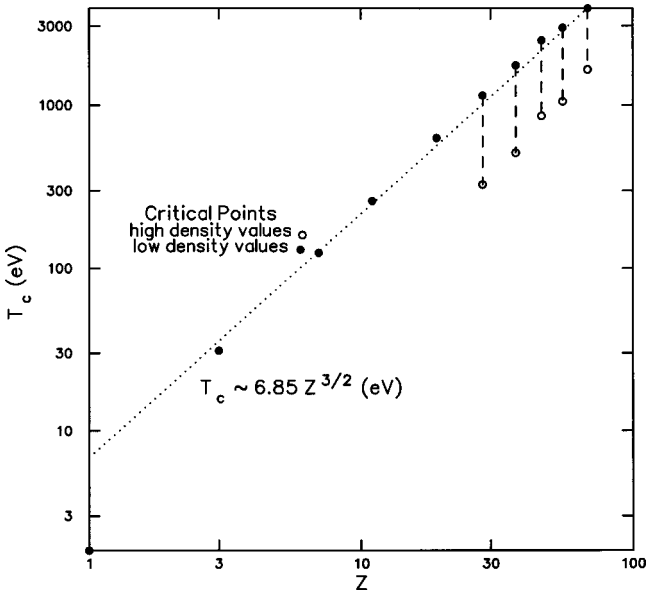

FIG. 11. The values of the critical-point temperature T_c vs the ion charge Z for a few selected elements. The dotted line shows the power law. The values for the two distinct critical points found for each element are connected by dashed lines.

been found for nickel and for all the elements studied with larger values of Z. I speculate that the occurrence of more than one critical point is related, crudely speaking, to the successive ionization of the various electron shells.

In Fig. 12, I plot the critical values of y_c, the ratio of the Coulomb energy to the thermal energy. This plot shows an interesting structure. The structure shown here can be interpreted to lend further support to the idea that the cellular model does reflect to some limited extent the known shell structure of the atoms. I emphasize that these effects are not put in artificially but follow from the solution of Eq. (3.15). In Fig. 13 I plot the critical values of the de Broglie density ζ_c. The low-density critical-point values trend upward and

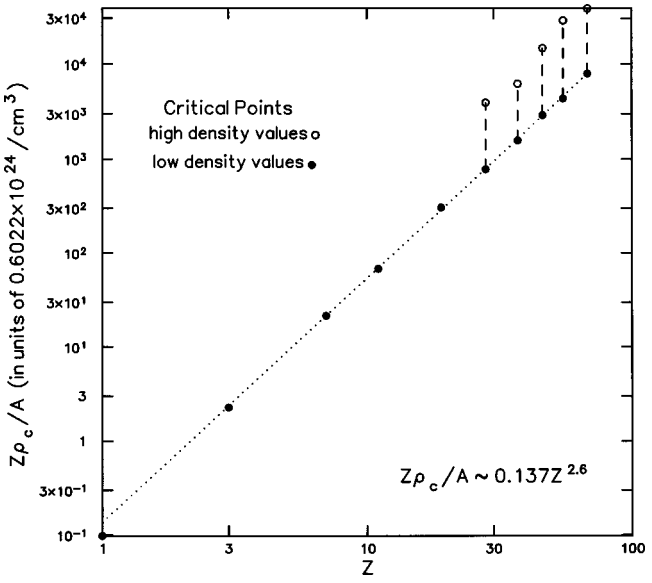

FIG. 10. The values of the critical-point electron density $Z\rho_c/\mathcal{A}$ vs the ion charge Z for a few selected elements. $\mathcal{A}$ is the gram atomic weight. The dotted line shows the power law. The values for the two distinct critical points found for each element are connected by dashed lines.

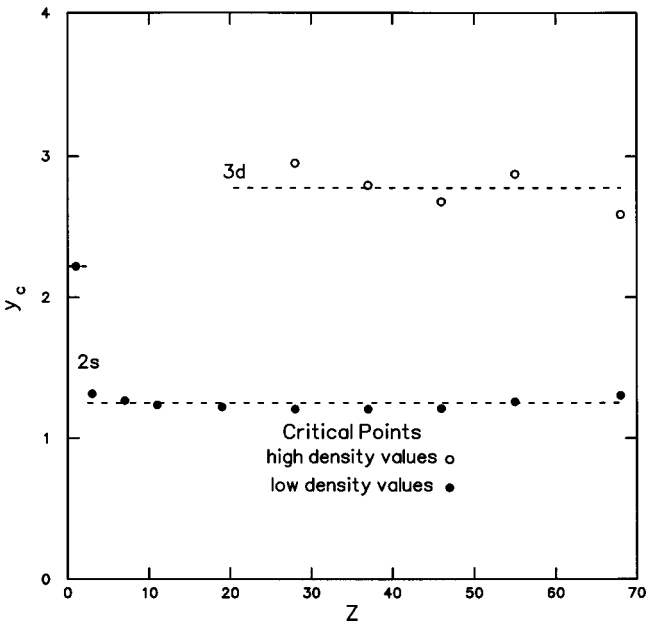

FIG. 12. The critical point values of y_c vs the ion charge Z for a few selected elements. It is to be noted that, for the low-density critical points, the value shifts from the hydrogen value ($1s$ electron shell) to a different value when the $2s$ electron shell begins to fill. At about the value of Z where the $3d$ electron shell begins to fill, the high-density critical points appear. The value of y_c remains relatively constant for both the high-density and the low-density critical points.

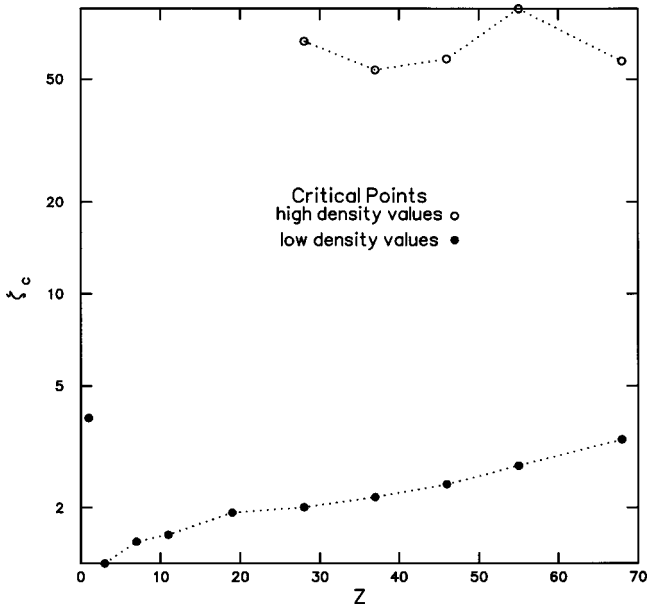

FIG. 13. The values of the critical-point de Broglie density ζ_c vs the ion charge Z for a few selected elements. The dotted lines connect values for the high- and low-density results. As ζ_c increases, the quantum effects become increasingly important.

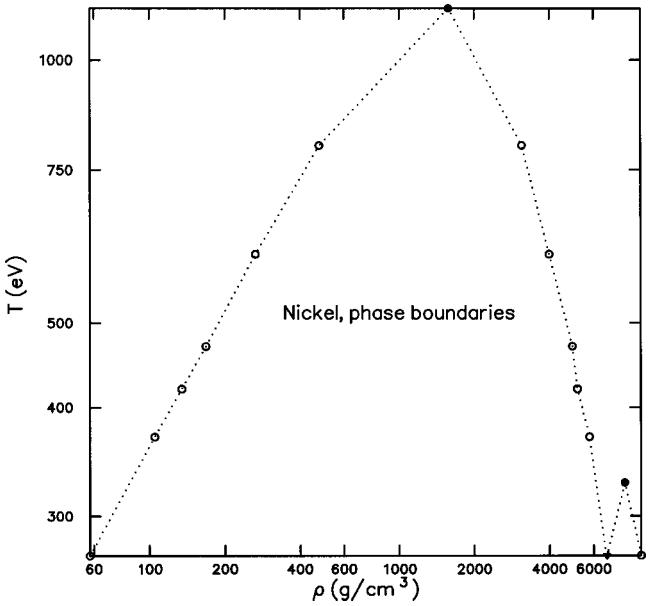

FIG. 14. The phase boundary of the spherical cellular model of nickel ($Z=28$) in the T-ρ plane. The solid dots are the two critical points and the open circles are the data points on the phase boundary. The discontinuities in slope result from the joining of the computed values by straight lines, except of course, at the triple point, marked by $\triangle$, where the two two-phase regions join.

reflect the increasing importance of quantum mechanics. The values for the high-density critical point are roughly constant and much larger than those for the low-density critical point. As a final remark, the lack of really smooth behavior is not surprising and presumably reflects to some degree the electronic shell structure of the atoms.

I list in Table I the critical-point values which I have determined for the spherical cellular model. The temperature is in eV, the density is in g/cm^3, and the pressure is in Mbars. The ratio $p_c\Omega_c/ZNkT_c$ relates to the law of corresponding states and is not completely constant. The ratio $Z\rho/\mathcal{A}$ is the electron density. In the cases where there are two critical points listed for an element, the values are listed in the same order for each of the various quantities.

I have computed the phase boundaries pendant to the critical points. A typical example is that for nickel as shown in Fig. 14. It is undoubtedly true that the behavior at the critical point is rounded and quadratic in form, however I

TABLE I. Critical-point values. T_c is in units of eV, ρ_c in g/cm^3, $\mathcal{A}$ is the gram atomic weight, p_c in Mbars, and $Z\rho_c/\mathcal{A}$ in units of 0.6022×10^{24}/cm^3.

Z	1, H	3, Li	7, N	11, Na	19, K	28, Ni	37, Rb	46, Pd	55, Cs	68, Er
T_c	1.83	31.0	124	260	632	1.14×10^3	1.74×10^3	2.46×10^3	2.93×10^3	3.84×10^3
						328	513	859	1.05×10^3	1.64×10^3
ρ_c	0.0986	5.27	43.1	143	631	1.58×10^3	3.65×10^3	6.74×10^3	1.06×10^4	1.96×10^4
						7.98×10^3	1.44×10^4	3.39×10^4	6.98×10^4	9.40×10^4
$\mathcal{A}$	1.00797	6.94	14.007	22.977	39.0963	56.71	85.4678	106.4	132.91	167.26
$\frac{p_c\Omega_c}{ZNkT_c}$	0.491	0.471	0.536	0.639	0.758	0.893	0.998	1.05	1.24	1.39
						0.552	0.346	0.832	1.30	0.696
p_c	8.96×10^{-2}	32.1	1.38×10^3	1.10×10^4	1.42×10^5	7.69×10^5	2.65×10^6	7.28×10^6	1.53×10^7	4.11×10^7
						6.88×10^5	1.07×10^6	1.01×10^7	3.82×10^7	4.22×10^7
y_c	2.22	1.32	1.27	1.24	1.22	1.21	1.21	1.21	1.26	1.30
						2.95	2.80	2.68	2.87	2.59
ζ_c	3.93	1.31	1.55	1.63	1.93	2.01	2.17	2.39	2.75	3.34
						66.2	53.6	58.1	84.3	57.2
$Z\rho_c/\mathcal{A}$	9.78×10^{-2}	2.28	21.6	68.6	307	780	1.57×10^3	2.91×10^3	4.36×10^3	7.97×10^3
						3.94×10^3	6.23×10^3	1.47×10^4	2.89×10^4	3.82×10^4

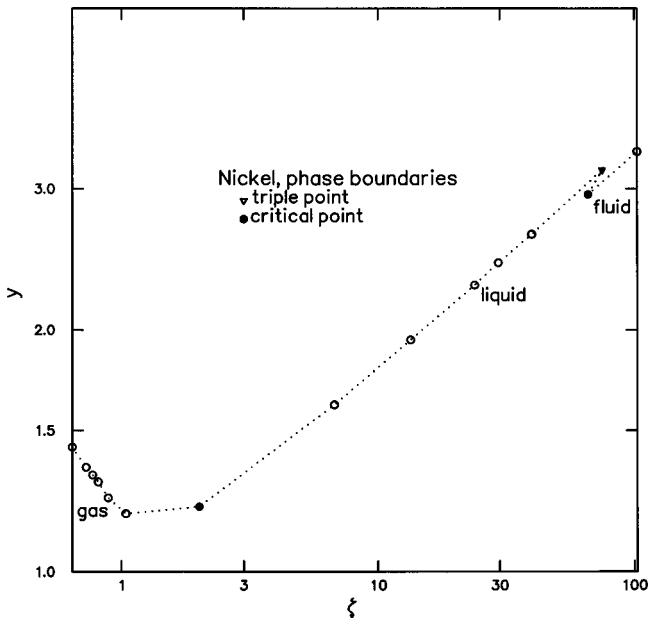

FIG. 15. The phase boundary of the spherical cellular model of nickel ($Z=28$) in the ζ-y plane. The solid dots are the two critical points, the open circles are the data points on the phase boundary, and the ∇ is a triple point.

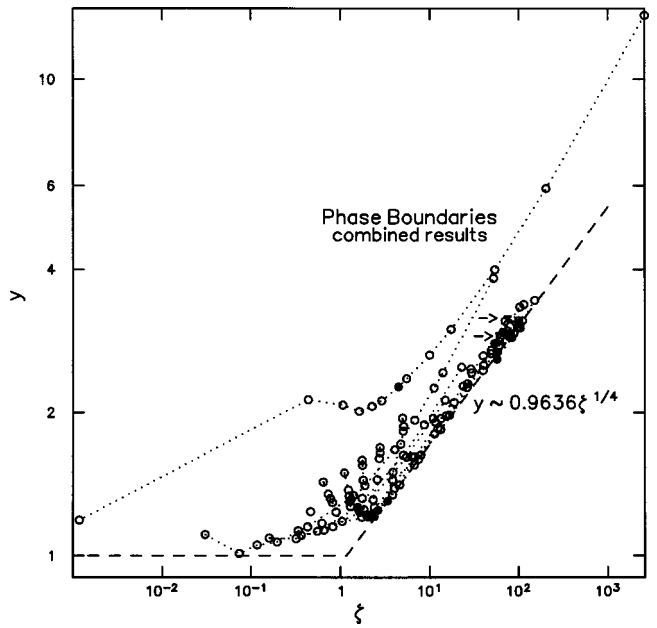

FIG. 16. The phase boundaries of the spherical cellular model for ten different elements. The critical points are solid circles and the data points are open circles. The triple points are upside down triangles. Since these triangles are a bit hard to locate, I have placed small arrows pointing towards them. The points corresponding to each element are joined by dotted lines. The dashed line has two parts: the first for smaller values of ζ is just $y=1$ and the second part is $y\sim 0.9636\zeta^{1/4}$ which appears to be a limit for the phase boundaries.

have connected the data points with straight lines. In this case there are two critical points plainly visible. The point where the two two-phase regions meet is the triple point as there are three different phases in equilibrium with each other at this special point. It turns out that it is somewhat more interesting to plot the phase boundaries in the y-ζ plane. I do this in Fig. 15. It is worth noticing that the phase boundary curve turns up for small values of ζ. This effect is more and more pronounced as Z increases. In Fig. 16 I plot all the phase boundary results. They appear to converge as Z increases to the limiting line shown in the figure for $\zeta \gtrsim 1$.

It appears from Fig. 16 that, except for hydrogen, the phase boundaries all terminate at some lower limiting value of ζ. Whether this behavior is definitive or not has not been resolved, owing to the rapid increase in computational time as lower densities are examined. In Fig. 17 I plot the pressure versus y for a constant value of ζ which is less than the apparent lower limit of ζ for the phase boundary of lithium. The electron pressure appears of decrease rather smoothly in a manner proportional to y^{-10}. For medium values of y, the rate to decrease slows as the model pressure increases above that of the ideal Fermi gas [22], This behavior argues that, at least for small ζ, there is no phase transition and the atom ionizes gradually and goes over smoothly to the fully ionized ideal Fermi gas, although as this point has not been thoroughly checked, I cannot be sure. For the smaller values of y, the pressure is within a few percent of the ideal Fermi gas values. For constant ζ, $y\propto\zeta^{1/3}/\rho^{1/6}$ and $y\propto\zeta^{1/6}/T^{1/4}$. Thus as $y\to\infty$ for fixed ζ, $T\to 0$ and $\rho\to 0$. Since by Eqs. (2.9) for small ζ and small y, $p\Omega/NkT\approx 1+Z$, I expect $p\propto(1+Z)\zeta^{8/3}y^{-10}$ as observed. When y is large, the system is cold and dilute. Thus only the center of mass motion would be expected to contribute to the pressure. In this case, the factor

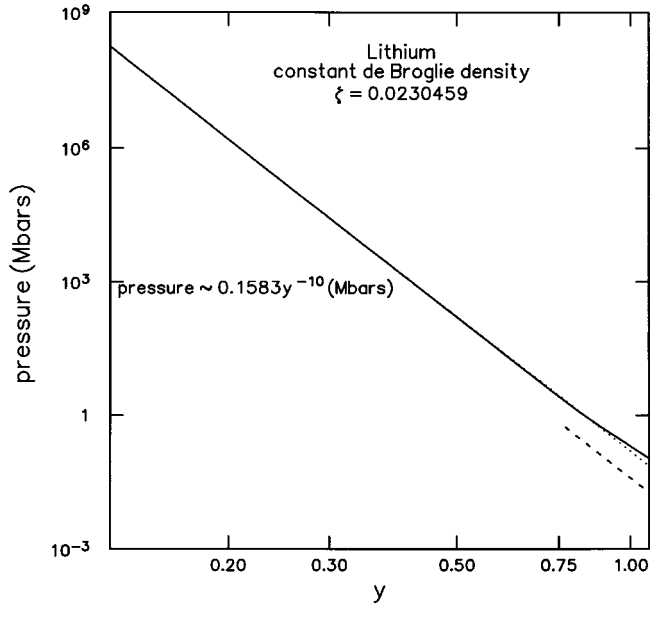

FIG. 17. The pressure for the spherical cellular model of lithium ($Z=3$) at a constant de Broglie density $\zeta=0.023\,045\,9$. The solid line is the spherical model result and the dotted line (mostly obscured by the solid line) is the formula shown. The short-dashed line is a continuation of the expected large y limiting behavior.

$(1+Z)$ would be replaced by 1. The extension of this asymptote is shown in Fig. 17. Excessive computing time has prevented the exploration of this region. Different behavior is expected and is illustrated for intermediate values of y.

I now turn to the question of the internal energy. However before doing so, it is appropriate to discuss thermodynamic consistency. The point at issue is the $\partial\epsilon_j/\partial T|_\Omega$ term which appears in Eq. (2.4). As we know from thermodynamics, given any of the usual thermodynamic quantities, we can construct the others in a thermodynamically consistent way. However, that is not the approach that is often taken, but rather what seems to be physically reasonable is used for, say, the pressure and the internal energy. In the case at hand, following that approach one would omit the $\partial\epsilon_j/\partial T|_\Omega$ term from the internal energy, which yields the physically reasonable energy

$$E=\sum_j \frac{\epsilon_j}{\exp[(\epsilon_j-\mu)/kT]+1}. \tag{5.2}$$

If one started from the ''physically reasonable'' internal energy, instead of using statistical mechanics to derive the Helmholtz free energy as I have done, then one would integrate Eq. (2.4) with respect to T to obtain the free energy and then use Eq. (2.5) to derive the pressure. In this case the Helmholtz free energy would become

$$A(\Omega,T)=\mathcal{N}\mu(\Omega,T) - kT\sum_j \ln(1+\exp\{[\mu(\Omega,T)-\epsilon_j]/(kT)\}) + T\int_T^\infty \sum_j \frac{\frac{1}{\tau}\frac{\partial\epsilon_j}{\partial\tau}\Big|_\Omega d\tau}{\exp[(\epsilon_j-\mu)/k\tau]+1}. \tag{5.3}$$

The corresponding pressure is

$$p\Omega=-\sum_k \left\{ \frac{\Omega\frac{\partial\epsilon_k}{\partial\Omega}\Big|_T}{\exp[(\epsilon_k-\mu)/kT]+1} - T\int_T^\infty \frac{\frac{\Omega}{\tau}\frac{\partial}{\partial\Omega}\left(\frac{\partial\epsilon_j}{\partial\tau}\Big|_\Omega\right)\Big|_\tau d\tau}{\exp[(\epsilon_j-\mu)/k\tau]+1} + T\int_T^\infty \frac{\frac{\Omega}{\tau}\frac{\partial\epsilon_j}{\partial\tau}\Big|_\Omega \frac{\partial}{\partial\Omega}\left[\frac{\epsilon_j-\mu}{k\tau}\right]\Big|_\tau \exp[(\epsilon_j-\mu)/k\tau]d\tau}{\{\exp[(\epsilon_j-\mu)/k\tau]+1\}^2} \right\}. \tag{5.4}$$

This approach is also worthwhile to investigate, but I shall not do so here.

The nub of the problem of thermodynamic consistency is the self-consistent potential. While the true physical potentials are independent of the temperature, the self-consistent potentials generally are not because they are based on the electron distribution. For very low temperatures, the electrons cluster around the ion, while for very high temperature, they are relatively uniformly distributed. This variation causes self-consistent potentials to be temperature dependent. A couple of examples are the Hartree or ''self-consistent field'' approximation [13], and the confined atom method [19,20].

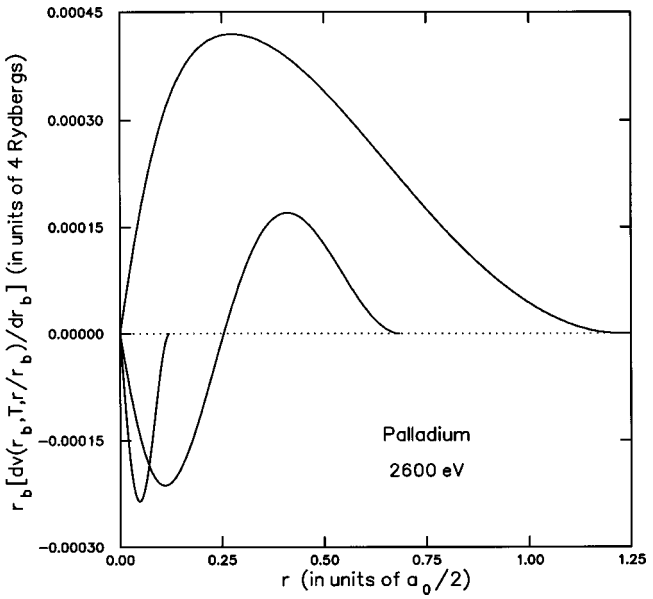

FIG. 18. Three $r_b\partial v(r_b,T,r/r_b)/\partial r_b$ vs r_b curves for different densities for the spherical cellular model of palladium ($Z=46$) at a temperature of 2600 eV. a_0 is the Bohr radius. The abscissa is in units of $a_0/2$ and the ordinate is in units of 4 Ry.

It may happen, as is the case with the Thomas-Fermi model [23], that the contribution of $\partial\epsilon_j/\partial T$ always cancels out and so need not be considered. The behavior of the $T\partial v/\partial T$ in the spherical, cellular model is apparently uniformly positive in the one-phase region and so cannot cancel, but does become relatively small for both large and small ζ. This feature can be understood physically by noticing that as the temperature increases the electrons tend towards a uniform distribution, rather than remaining clustered about the ion. This feature causes electrons to move away from the ion thus increasing v.

The function $r_b\partial v/\partial r_b$ shows more interesting behavior as illustrated in Fig. 18. For low densities (that curve extends to larger values of r) the electrons move away from the central ion to take advantage of the extra available room leading to an increase in v. On the other hand, for high densities, the electrons relax from the relatively uniform distribution forced on them by the Pauli principle to be somewhat more clustered around the central ion. This behavior results in a smaller v, as shown in Fig. 18. For intermediate densities, a combination of these two behaviors is illustrated in that figure.

A typical illustration of the energy for the temperature greater than the critical temperature is shown for lithium in Fig. 19. In this figure I display both the thermodynamically consistent internal energy, and what would be expected to be the physically reasonable energy. In this case these two energies differ. For both large and small values of ζ, the difference tends to zero. For intermediate values of ζ the dif-

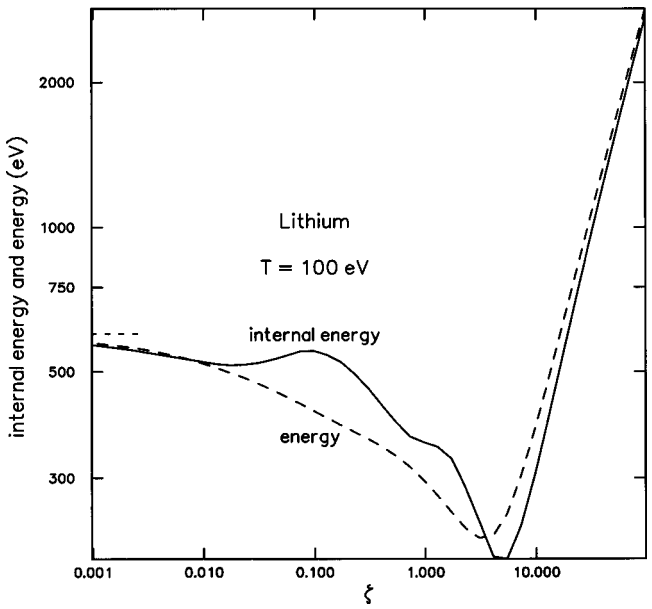

FIG. 19. The "physically reasonable" energy (labeled energy) and the internal energy vs the de Broglie density for the spherical cellular model of lithium ($Z=3$) at a temperature of 100 eV. The short-dashed line is the low-density, total-ionization limit.

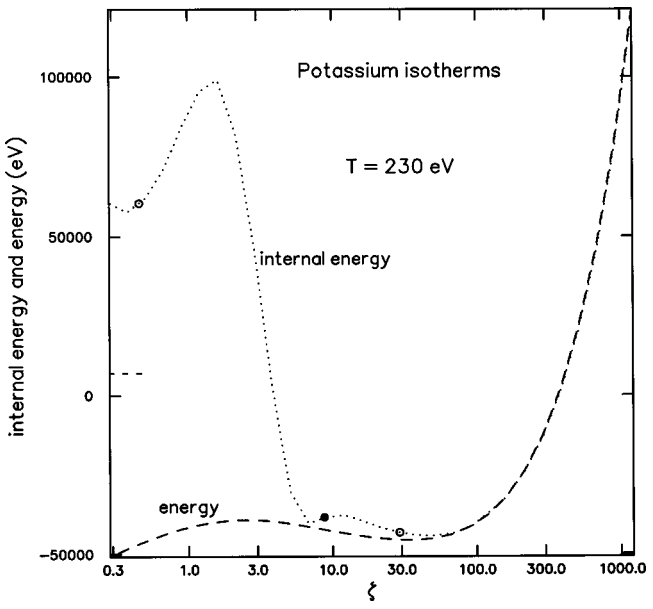

FIG. 20. The physically reasonable energy (labeled energy) and the internal energy vs the de Broglie density for the spherical cellular model of potassium ($Z=19$) at a temperature of 230 eV. The open circles represent the phase boundaries for this temperature. The solid circle represents the critical-point value of ζ. The short-dashed line is the low-density, total-ionization limit.

ference can be quite significant.

In Fig. 20 I illustrate the behavior of the energies along an isotherm which passes through the two-phase region. In this case, the energy and the internal energy have rather different values in the lower-density phase, although, as was the case for a temperature above the critical temperature, they both are substantially equal in the higher-density phase. I expect that in the low-density limit both the energy and internal energy will tend to the low-density, total-ionization limit.

The internal energy relates to the total-ionization energy in the following way. First, as the temperature is not zero, there will be some ionization, so this effect tends to increase the internal energy above the total-ionization energy. Second, the boundary conditions, Eq. (3.9), permit a lower energy than that of a free atom. These two features make the comparison of the spherical cellular model internal energies with the experimental values of the total-ionization energy as given by Moore [24] difficult, and will not be attempted here.

ACKNOWLEDGMENT

The author would like to acknowledge a number of helpful conversations with J. D. Johnson.

APPENDIX A: COMPUTATION OF THE DERIVATIVES

First I define the quantities

$$V_\nu(l,\lambda)=\frac{e^2}{r_b}Z^{-1/3}\langle\phi_{l,\nu}(r_b,\vec{\rho})|v(r_b,T,\rho)\rho^{-1}|\phi_{l,\lambda}(r_b,\vec{\rho})\rangle,\quad H_\nu(l,\lambda)=\frac{e^2}{r_b}\langle\phi_{l,\nu}(r_b,\vec{\rho})|\rho^2|\phi_{l,\lambda}(r_b,\vec{\rho})\rangle,$$

$$W_\nu(l,\lambda)=\frac{e^2}{r_b}Z^{-1/3}\langle\phi_{l,\nu}|\frac{r_b v'(r_b,T,\rho)}{\rho}|\phi_{l,\lambda}\rangle,\quad U_\nu(l,\lambda)=\frac{e^2}{r_b}Z^{-1/3}\langle\phi_{l,\nu}|\frac{T\dot{v}(r_b,T,\rho)}{\rho}|\phi_{l,\lambda}\rangle,$$

$$V_{\mathrm{ion},\nu}(l,\lambda)=\frac{e^2}{r_b}Z^{2/3}\langle\phi_{l,\nu}(r_b,\vec{\rho})|\rho^{-1}|\phi_{l,\lambda}(r_b,\vec{\rho})\rangle, \tag{A1}$$

and the further quantities

$$\mathcal{A}(l,\lambda)=\sum_{\nu\neq\lambda}\frac{[V_\nu(l,\lambda)]^2}{\mathcal{E}_{l,\nu}-\mathcal{E}_{l,\lambda}},\quad \mathcal{B}(l,\lambda)=\sum_{\nu\neq\lambda}\frac{[H_\nu(l,\lambda)]^2}{\mathcal{E}_{l,\nu}-\mathcal{E}_{l,\lambda}},\quad \mathcal{C}(l,\lambda)=\sum_{\nu\neq\lambda}\frac{V_\nu(l,\lambda)H_\nu(l,\lambda)}{\mathcal{E}_{l,\nu}-\mathcal{E}_{l,\lambda}},$$

$$\mathcal{F}(l,\lambda)=\sum_{\nu\neq\lambda}\frac{V_\nu(l,\lambda)W_\nu(l,\lambda)}{\mathcal{E}_{l,\nu}-\mathcal{E}_{l,\lambda}},\quad \mathcal{G}(l,\lambda)=\sum_{\nu\neq\lambda}\frac{H_\nu(l,\lambda)W_\nu(l,\lambda)}{\mathcal{E}_{l,\nu}-\mathcal{E}_{l,\lambda}}, \tag{A2}$$

$$\Theta(l,\lambda)=\sum_{\nu\neq\lambda}\frac{V_\nu(l,\lambda)U_\nu(l,\lambda)}{\mathcal{E}_{l,\nu}-\mathcal{E}_{l,\lambda}},\quad \Gamma(l,\lambda)=\sum_{\nu\neq\lambda}\frac{H_\nu(l,\lambda)U_\nu(l,\lambda)}{\mathcal{E}_{l,\nu}-\mathcal{E}_{l,\lambda}},$$

$$\mathcal{A}_{\rm ion}(l,\lambda)=\sum_{\nu\neq\lambda}\frac{V_{{\rm ion},\nu}(l,\lambda)V_\nu(l,\lambda)}{\mathcal{E}_{l,\nu}-\mathcal{E}_{l,\lambda}},\quad \mathcal{C}_{\rm ion}(l,\lambda)=\sum_{\nu\neq\lambda}\frac{V_{{\rm ion},\nu}(l,\lambda)H_\nu(l,\lambda)}{\mathcal{E}_{l,\nu}-\mathcal{E}_{l,\lambda}},$$

$$\mathcal{F}_{\rm ion}(l,\lambda)=\sum_{\nu\neq\lambda}\frac{V_{{\rm ion},\nu}(l,\lambda)W_\nu(l,\lambda)}{\mathcal{E}_{l,\nu}-\mathcal{E}_{l,\lambda}},\quad \Theta_{\rm ion}(l,\lambda)=\sum_{\nu\neq\lambda}\frac{V_{{\rm ion},\nu}(l,\lambda)U_\nu(l,\lambda)}{\mathcal{E}_{l,\nu}-\mathcal{E}_{l,\lambda}}.$$

To compute the last terms in Eqs. (3.23) and (3.24), I need the derivative of the wave function

$$Z^{-1/3}r_b\frac{\partial\phi_{l,\lambda}(r_b,\vec{\rho})}{\partial r_b}=\sum_{\nu\neq\lambda}\frac{\phi_{l,\nu}(r_b,\vec{\rho})}{\mathcal{E}_{l,\nu}-\mathcal{E}_{l,\lambda}}\left\{\left(1+\frac{\partial\ln m^*}{\partial\ln r_b}\right)V_\nu(l,\lambda)+W_\nu(l,\lambda)\right.$$
$$\left.+\frac{1}{2}Z^{-1/3}\left[\left(1+\frac{\partial\ln m^*}{\partial\ln r_b}\right)F\left(\frac{y^2}{Z}\right)-\frac{y^2}{Z}F'\left(\frac{y^2}{Z}\right)\right]H_\nu(l,\lambda)\right\}. \tag{A3}$$

Using Eq. (A3) I obtain, for the needed case $\vec{k}=\vec{0}$ where V and H are real, the result

$$Z^{-1/3}r_b\frac{\partial}{\partial r_b}\langle\phi_{l,\lambda}(\vec{r})|\left[-\frac{1}{2}\left(1-\frac{m^*}{m}\right)\frac{e^2v(r_b,T,r/r_b)}{r}+\frac{m^*e^2r^2}{4mr_b^3}F\left(\frac{y^2}{Z}\right)\right]|\phi_{l,\lambda}(\vec{r})\rangle=\left(1+\frac{\partial\ln m^*}{\partial\ln r_b}\right)\left(\frac{m^*}{m}-1\right)\mathcal{A}(l,\lambda)$$
$$+\frac{1}{2}Z^{-2/3}\left[\left(1+\frac{\partial\ln m^*}{\partial\ln r_b}\right)F\left(\frac{y^2}{Z}\right)-\frac{y^2}{Z}F'\left(\frac{y^2}{Z}\right)\right]\frac{m^*}{m}F\left(\frac{y^2}{Z}\right)\mathcal{B}(l,\lambda)+Z^{-1/3}\left\{\left(1+\frac{\partial\ln m^*}{\partial\ln r_b}\right)\frac{m^*}{m}F\left(\frac{y^2}{Z}\right)+\frac{1}{2}\left(\frac{m^*}{m}-1\right)\right.$$
$$\left.\times\left[\left(1+\frac{\partial\ln m^*}{\partial\ln r_b}\right)F\left(\frac{y^2}{Z}\right)-\frac{y^2}{Z}F'\left(\frac{y^2}{Z}\right)\right]\right\}\mathcal{C}(l,\lambda)-\left(1-\frac{m^*}{m}\right)\mathcal{F}(l,\lambda)+\frac{m^*}{2m}Z^{-1/3}F\left(\frac{y^2}{Z}\right)\mathcal{G}(l,\lambda)+\frac{1}{2}\left(1-\frac{m*}{m}\right)V_\lambda(l,\lambda)$$
$$+\frac{1}{2m}\frac{\partial m^*}{\partial\ln r_b}\left[V_\lambda(l,\lambda)+\frac{1}{2}Z^{-1/3}F\left(\frac{y^2}{Z}\right)H_\lambda(l,\lambda)\right]-\frac{m^*}{4m}Z^{-1/3}\left[F\left(\frac{y^2}{Z}\right)+\frac{y^2}{Z}F'\left(\frac{y^2}{Z}\right)\right]H_\lambda(l,\lambda)-\frac{1}{2}\left(1-\frac{m^*}{m}\right)W_\lambda(l,\lambda), \tag{A4}$$

for parallel spins. For antiparallel spins I get

$$Z^{-1/3}r_b\frac{\partial}{\partial r_b}\langle\phi_{l,\lambda}(\vec{r})|\frac{e^2r^2}{4r_b^3}F\left(\frac{y^2}{Z}\right)|\phi_{l,\lambda}(\vec{r})\rangle=\frac{1}{2}Z^{-2/3}\left[F\left(\frac{y^2}{Z}\right)-\frac{y^2}{Z}F'\left(\frac{y^2}{Z}\right)\right]F\left(\frac{y^2}{Z}\right)\mathcal{B}(l,\lambda)+Z^{-1/3}F\left(\frac{y^2}{Z}\right)\mathcal{C}(l,\lambda)$$
$$+Z^{-1/3}\frac{1}{2}F\left(\frac{y^2}{Z}\right)\mathcal{G}(l,\lambda)-\frac{1}{4}Z^{-1/3}\left[F\left(\frac{y^2}{Z}\right)+\frac{y^2}{Z}F'\left(\frac{y^2}{Z}\right)\right]H_\lambda(l,\lambda). \tag{A5}$$

In addition I need

$$\frac{e^2}{Z^{1/3}r_b}\langle\phi_{l,\lambda}(\vec{r})|\frac{Z}{r/r_b}-\frac{v(r_b,T,r/r_b)}{r/r_b}|\phi_{l,\lambda}(\vec{r})\rangle=V_{{\rm ion},\lambda}(l,\lambda)-V_\lambda(l,\lambda),$$

$$\frac{e^2}{Z^{1/3}r_b}r_b\frac{\partial}{\partial r_b}\langle\phi_{l,\lambda}(\vec{r})|\frac{Z}{r/r_b}-\frac{v(r_b,T,r/r_b)}{r/r_b}|\phi_{l,\lambda}(\vec{r})\rangle$$
$$=-W_\lambda(l,\lambda)+2\left\{\left(1+\frac{\partial\ln m^*}{\partial\ln r_b}\right)[\mathcal{A}_{\rm ion}(l,\lambda)-\mathcal{A}(l,\lambda)]+\mathcal{F}_{\rm ion}(l,\lambda)-\mathcal{F}(l,\lambda)\right.$$
$$\left.+\frac{1}{2}Z^{-1/3}\left[\left(1+\frac{\partial\ln m^*}{\partial\ln r_b}\right)F\left(\frac{y^2}{Z}\right)-\frac{y^2}{Z}F'\left(\frac{y^2}{Z}\right)\right][\mathcal{C}_{\rm ion}(l,\lambda)-\mathcal{C}(l,\lambda)]\right\}, \tag{A6}$$

for parallel spins. For antiparallel spins I get

$$\frac{e^2}{Z^{1/3}r_b}r_b\frac{\partial}{\partial r_b}\langle\phi_{l,\lambda}(\vec{r})|\frac{Z}{r/r_b}-\frac{v(r_b,T,r/r_b)}{r/r_b}|\phi_{l,\lambda}(\vec{r})\rangle$$
$$=W_\lambda(l,\lambda)+2\left\{\mathcal{A}_{\rm ion}(l,\lambda)-\mathcal{A}(l,\lambda)+\mathcal{F}_{\rm ion}(l,\lambda)-\mathcal{F}(l,\lambda)+\frac{1}{2}Z^{-1/3}\left[F\left(\frac{y^2}{Z}\right)-\frac{y^2}{Z}F'\left(\frac{y^2}{Z}\right)\right][\mathcal{C}_{\rm ion}(l,\lambda)-\mathcal{C}(l,\lambda)]\right\}. \tag{A7}$$

The next ingredient that I need is

$$T\frac{\partial\phi_{l,\lambda}(r_b,\vec{\rho})}{\partial T}=\sum_{\nu\neq\lambda}\frac{\phi_{l,\nu}(r_b,\vec{\rho})}{\mathcal{E}_{l,\nu}-\mathcal{E}_{l,\lambda}}\left\{\frac{\partial\ln m^*}{\partial\ln T}\left[V_\nu(l,\lambda)+\frac{1}{2}Z^{-1/3}F\left(\frac{y^2}{Z}\right)H_\nu(l,\lambda)\right]+U_\nu(l,\lambda)-\frac{1}{2}Z^{-1/3}\frac{y^2}{Z}F'\left(\frac{y^2}{Z}\right)H_\nu(l,\lambda)\right\} \tag{A8}$$

in order that I may compute

$$Z^{-1/3}T\frac{\partial}{\partial T}\langle\phi_{l,\lambda}(\vec{r})|\left\{-\frac{1}{2}\left(1-\frac{m^*}{m}\right)\frac{e^2v(r_b,T,r/r_b)}{r}+\frac{m^*}{4m}\frac{e^2r^2}{r_b^3}F\left(\frac{y^2}{Z}\right)\right\}|\phi_{l,\lambda}(\vec{r})\rangle$$
$$=\frac{\partial\ln m^*}{\partial\ln T}\left(\frac{m^*}{m}-1\right)\mathcal{A}(l,\lambda)+\frac{1}{2}Z^{-2/3}\left[\frac{\partial\ln m^*}{\partial\ln T}F\left(\frac{y^2}{Z}\right)-\frac{y^2}{Z}F'\left(\frac{y^2}{Z}\right)\right]F\left(\frac{y^2}{Z}\right)\mathcal{B}(l,\lambda)+Z^{-1/3}\left[\left(\frac{m^*}{m}+1\right)\frac{\partial\ln m^*}{\partial\ln T}F\left(\frac{y^2}{Z}\right)\right.$$
$$\left.-\left(\frac{m^*}{m}-1\right)\frac{y^2}{Z}F'\left(\frac{y^2}{Z}\right)\right]\mathcal{C}(l,\lambda)-\left(1-\frac{m^*}{m}\right)\Theta(l,\lambda)+\frac{m^*}{2m}Z^{-1/3}F\left(\frac{y^2}{Z}\right)\Gamma(l,\lambda)-\frac{1}{2}\left(1-\frac{m^*}{m}\right)U_\lambda(l,\lambda)$$
$$+\frac{1}{2m}\frac{\partial m^*}{\partial\ln T}\left[V_\lambda(l,\lambda)+\frac{1}{2}Z^{-1/3}F\left(\frac{y^2}{Z}\right)H_\lambda(l,\lambda)\right]-\frac{m^*}{4m}Z^{-1/3}\frac{y^2}{Z}F'\left(\frac{y^2}{Z}\right)H_\lambda(l,\lambda). \tag{A9}$$

For the antiparallel case, I get

$$Z^{-1/3}T\frac{\partial}{\partial T}\langle\phi_{l,\lambda}(\vec{r})|\frac{e^2r^2}{4r_b^3}F\left(\frac{y^2}{Z}\right)|\phi_{l,\lambda}(\vec{r})\rangle$$
$$=-\frac{1}{2}Z^{-2/3}\frac{y^2}{Z}F'\left(\frac{y^2}{Z}\right)F\left(\frac{y^2}{Z}\right)\mathcal{B}(l,\lambda)+\frac{1}{2}Z^{-1/3}F\left(\frac{y^2}{Z}\right)\Gamma(l,\lambda)-\frac{1}{4}Z^{-1/3}\frac{y^2}{Z}F'\left(\frac{y^2}{Z}\right)H_\lambda(l,\lambda). \tag{A10}$$

In addition I need the results

$$-\frac{e^2}{2Z^{1/3}r_b}T\frac{\partial}{\partial T}\langle\phi_{l,\lambda}(\vec{r})|\frac{Z}{r/r_b}-\frac{v(r_b,T,r/r_b)}{r/r_b}|\phi_{l,\lambda}(\vec{r})\rangle$$
$$=\frac{e^2}{2r_b}U_\lambda(l,\lambda)-\frac{e^2}{r_b}\left\{\frac{\partial\ln m*}{\partial\ln T}\left[\mathcal{A}_{\rm ion}(l,\lambda)-\mathcal{A}(l,\lambda)+\frac{1}{2}Z^{-1/3}F\left(\frac{y^2}{Z}\right)[\mathcal{C}_{\rm ion}(l,\lambda)-\mathcal{C}(l,\lambda)]\right]\right.$$
$$\left.+\Theta_{\rm ion}(l,\lambda)-\Theta(l,\lambda)-\frac{1}{2}Z^{-1/3}\frac{y^2}{Z}F'\left(\frac{y^2}{Z}\right)[\mathcal{C}_{\rm ion}(l,\lambda)-\mathcal{C}(l,\lambda)]\right\}, \tag{A11}$$

for parallel spins and for antiparallel,

$$-\frac{e^2}{2Z^{1/3}r_b}T\frac{\partial}{\partial T}\langle\phi_{l,\lambda}(\vec{r})|\frac{Z}{r/r_b}-\frac{v(r_b,T,r/r_b)}{r/r_b}|\phi_{l,\lambda}(\vec{r})\rangle$$
$$=\frac{e^2}{2r_b}U_\lambda(l,\lambda)-\frac{e^2}{r_b}\left\{\Theta_{\rm ion}(l,\lambda)-\Theta(l,\lambda)-\frac{1}{2}Z^{-1/3}\frac{y^2}{Z}F'\left(\frac{y^2}{Z}\right)[\mathcal{C}_{\rm ion}(l,\lambda)-\mathcal{C}(l,\lambda)]\right\}. \tag{A12}$$

A discussion of the actual computation of v' and $\dot{v}$ will be deferred to the end of this appendix. The quantities W, U, $\mathcal{F}$, $\mathcal{F}_{\rm ion}$, $\mathcal{G}$, Θ, $\Theta_{\rm ion}$, and Γ, which were defined above depend on these derivatives. They may be computed from a knowledge of these derivatives and the functions

$$V_{\rm proto}(r)=\sum_{l,\lambda}\left(\frac{3}{2}-\frac{m^*(\lambda)}{2m}\right)\int d\vec{k}\sum_{\nu\neq\lambda}\frac{(2l+1)\phi^*_{l,\nu}(r)\phi_{l,\lambda}(r)r^2V_\nu(l,\lambda)}{(\mathcal{E}_{l,\nu}-\mathcal{E}_{l,\lambda})(\exp\{[\epsilon_{l,\lambda}(\vec{k})-\mu]/kT\}+1)},$$

$$H_{\rm proto}(r)=\sum_{l,\lambda}\frac{m^*(\lambda)}{m}\int d\vec{k}\sum_{\nu\neq\lambda}\frac{(2l+1)\phi^*_{l,\nu}(r)\phi_{l,\lambda}(r)r^2H_\nu(l,\lambda)}{(\mathcal{E}_{l,\nu}-\mathcal{E}_{l,\lambda})(\exp\{[\epsilon_{l,\lambda}(\vec{k})-\mu]/kT\}+1)}, \tag{A13}$$

$$I_{\rm proto}(r)=\sum_{l,\lambda}\frac{1}{2}\left(1+\frac{m^*(\lambda)}{m}\right)\int d\vec{k}\sum_{\nu\neq\lambda}\frac{(2l+1)\phi^*_{l,\nu}(r)\phi_{l,\lambda}(r)r^2V_{{\rm ion},\nu}(l,\lambda)}{(\mathcal{E}_{l,\nu}-\mathcal{E}_{l,\lambda})(\exp\{[\epsilon_{l,\lambda}(\vec{k})-\mu]/k\}+1)}.$$

Thus I may compute

$$\sum_{l,\lambda}\int d\vec{k}\frac{[3-m^*(\lambda)/m](2l+1)W_\lambda(l,\lambda)}{4(\exp\{[\epsilon_{l,\lambda}(\vec{k})-\mu]/kT\}+1)}=e^2Z^{-1/3}\int_0^{r_b}dr\left(\frac{3}{4}\mathcal{D}(r_b,T,r/r_b)-\frac{1}{4}\mathcal{D}^*(r_b,T,r/r_b)\right)r_bv'(r_b,T,r/r_b)/r,$$

$$\sum_{l,\lambda}\int d\vec{k}\frac{[3-m^*(\lambda)/m](2l+1)U_\lambda(l,\lambda)}{4(\exp\{[\epsilon_{l,\lambda}(\vec{k})-\mu]/kT\}+1)}=e^2Z^{-1/3}\int_0^{r_b}dr\left(\frac{3}{4}\mathcal{D}(r_b,T,r/r_b)-\frac{1}{4}\mathcal{D}^*(r_b,T,r/r_b)\right)T\dot{v}(r_b,T,r/r_b)/r,$$

$$\sum_{l,\lambda}\int d\vec{k}\frac{[3-m^*(\lambda)/m](2l+1)\mathcal{F}(l,\lambda)}{2(\exp\{[\epsilon_{l,\lambda}(\vec{k})-\mu]/kT\}+1)}=e^2Z^{-1/3}\int_0^{r_b}drV_{\rm proto}(r)r_bv'(r_b,T,r/r_b)/r,$$

$$\sum_{l,\lambda}\int d\vec{k}\frac{[1+m^*(\lambda)/m](2l+1)\mathcal{F}_{\rm ion}(l,\lambda)}{2(\exp\{[\epsilon_{l,\lambda}(\vec{k})-\mu]/kT\}+1)}=e^2Z^{-1/3}\int_0^{r_b}drI_{\rm proto}(r)r_bv'(r_b,T,r/r_b)/r,$$

$$\sum_{l,\lambda}\int d\vec{k}\frac{m^*(\lambda)(2l+1)\mathcal{G}(l,\lambda)}{m(\exp\{[\epsilon_{l,\lambda}(\vec{k})-\mu]/kT\}+1)}=e^2Z^{-1/3}\int_0^{r_b}drH_{\rm proto}(r)r_bv'(r_b,T,r/r_b)/r,$$

$$\sum_{l,\lambda}\int d\vec{k}\frac{[3-m^*(\lambda)/m](2l+1)\Theta(l,\lambda)}{2(\exp\{[\epsilon_{l,\lambda}(\vec{k})-\mu]/kT\}+1)}=e^2Z^{-1/3}\int_0^{r_b}drV_{\rm proto}(r)T\dot{v}(r_b,T,r/r_b)/r,$$

$$\sum_{l,\lambda}\int d\vec{k}\frac{[1+m^*(\lambda)/m](2l+1)\Theta_{\rm ion}(l,\lambda)}{2(\exp\{[\epsilon_{l,\lambda}(\vec{k})-\mu]/kT\}+1)}=e^2Z^{-1/3}\int_0^{r_b}drI_{\rm proto}(r)T\dot{v}(r_b,T,r/r_b)/r,$$

$$\sum_{l,\lambda}\int d\vec{k}\frac{m^*(\lambda)(2l+1)\Gamma(l,\lambda)}{m(\exp\{[\epsilon_{l,\lambda}(\vec{k})-\mu]/kT\}+1)}=e^2Z^{-1/3}\int_0^{r_b}drH_{\rm proto}(r)T\dot{v}(r_b,T,r/r_b)/r. \tag{A14}$$

It is useful to collect the terms which contribute to the pressure and to the internal energy which involve $r_b\partial v/\partial r_r$ and $T\partial v/\partial T$. The corrections to the pressure and the internal energy on this account are

$$\Delta p=\frac{202.3023}{x_0^3}\sum_{l,\lambda}\int d\vec{k}\frac{\mathcal{P}(l,\lambda)}{\exp\{[\epsilon_{l,\lambda}(\vec{k})-\mu]/kT\}+1}=\frac{202.3023}{x_0^3}e^2Z^{-1/3}\left\{\int_0^{r_b}dr\left(\frac{3}{4}\mathcal{D}(r_b,T,r/r_b)-\frac{1}{4}\mathcal{D}^*(r_b,T,r/r_b)\right)\right.$$
$$\times r_bv'(r_b,T,r/r_b)/r+\int_0^{r_b}dr[V_{\rm proto}(r)+I_{\rm proto}(r)]r_bv'(r_b,T,r/r_b)/r$$
$$\left.-\frac{Z^{-1/3}}{2}F\left(\frac{y^2}{Z}\right)\int_0^{r_b}drH_{\rm proto}(r)r_bv'(r_b,T,r/r_b)/r\right\},$$

$$\Delta u=\sum_{l,\lambda}\int d\vec{k}\frac{\mathcal{U}(l,\lambda)}{\exp\{[\epsilon_{l,\lambda}(\vec{k})-\mu]/kT\}+1}=e^2Z^{-1/3}\left\{\int_0^{r_b}dr\left(\frac{3}{4}\mathcal{D}(r_b,T,r/r_b)-\frac{1}{4}\mathcal{D}^*(r_b,T,r/r_b)\right)T\dot{v}(r_b,T,r/r_b)/r\right.$$
$$\left.+\int_0^{r_b}dr[V_{\rm proto}(r)+I_{\rm proto}(r)]T\dot{v}(r_b,T,r/r_b)/r-\frac{Z^{-1/3}}{2}F\left(\frac{y^2}{Z}\right)\int_0^{r_b}drH_{\rm proto}(r)T\dot{v}(r_b,T,r/r_b)/r\right\}, \tag{A15}$$

where

$$\mathcal{P}(l,\lambda)=\left(\frac{3}{4}-\frac{m^*(\lambda)}{4m}\right)W_\lambda(l,\lambda)+\frac{1}{2}\left(1+\frac{m^*(\lambda)}{m}\right)\mathcal{F}_{\rm ion}(l,\lambda)+\left(\frac{1}{2}-\frac{3m^*(\lambda)}{2m}\right)\mathcal{F}(l,\lambda)-\frac{m^*(\lambda)}{2m}Z^{-1/3}F\left(\frac{y^2}{Z}\right)\mathcal{G}(l,\lambda),$$

$$\mathcal{U}(l,\lambda)=\left(\frac{3}{4}-\frac{m^*(\lambda)}{4m}\right)U_\lambda(l,\lambda)+\frac{1}{2}\left(1+\frac{m^*(\lambda)}{m}\right)\Theta_{\rm ion}(l,\lambda)+\left(\frac{1}{2}-\frac{3m^*(\lambda)}{2m}\right)\Theta(l,\lambda)-\frac{m^*(\lambda)}{2m}Z^{-1/3}F\left(\frac{y^2}{Z}\right)\Gamma(l,\lambda). \tag{A16}$$

The derivatives of $v(r_b,T,r/r_b)$ are

$$r_b v'(r_b,T,r/r_b)=\left(\frac{Z-1}{Z}\right)r_b\int_{(r/r_b)}^1\left(1-\frac{r}{\beta r_b}\right)[\mathcal{D}(r_b,T,\beta)+r_b\mathcal{D}'(r_b,T,\beta)]d\beta,$$

$$T\dot v(r_b,T,r/r_b)=\left(\frac{Z-1}{Z}\right)r_b\int_{(r/r_b)}^1\left(1-\frac{r}{\beta r_b}\right)\times T\dot{\mathcal{D}}(r_b,T,\beta)d\beta. \tag{A17}$$

In order to compute the derivatives of $\mathcal{D}$ I will need

$$r_b\mu'(r_b,T)=\sum_{l,\lambda}\frac{r_b\frac{\partial\epsilon_{l,\lambda}}{\partial r_b}\exp[(\epsilon_{l,\lambda}-\mu)/kT]}{\{\exp[(\epsilon_{l,\lambda}-\mu)/kT]+1\}^2}\times\left[\sum_{l,\lambda}\frac{\exp[(\epsilon_{l,\lambda}-\mu)/kT]}{\{\exp[(\epsilon_{l,\lambda}-\mu)/kT]+1\}^2}\right]^{-1}, \tag{A18}$$

$$T\dot\mu(r_b,T)=\sum_{l,\lambda}\frac{\left\{T\frac{\partial\epsilon_{l,\lambda}}{\partial T}-\epsilon_{l,\lambda}+\mu\right\}\exp[(\epsilon_{l,\lambda}-\mu)/kT]}{\{\exp[(\epsilon_{l,\lambda}-\mu)/kT]+1\}^2}\times\left[\sum_{l,\lambda}\frac{\exp[(\epsilon_{l,\lambda}-\mu)/kT]}{\{\exp[(\epsilon_{l,\lambda}-\mu)/kT]+1\}^2}\right]^{-1}.$$

Equations (A18) together with Eqs. (3.23)–(3.25), (3.27)–(3.29), and (A3) complete the ingredients that I need to compute $\mathcal{D}'$ and $\dot{\mathcal{D}}$:

$$r_b\mathcal{D}'(r_b,T,r/r_b)=2\sum_{l,\lambda}\frac{(2l+1)\phi^*_{l,\lambda}(r)\left[\phi_{l,\lambda}(r)+r_b\frac{\partial\phi_{l,\lambda}(r)}{\partial r_b}\right]r^2}{\exp[(\epsilon_{l,\lambda}-\mu)/kT]+1}-\sum_{l,\lambda}\frac{(2l+1)\phi^*_{l,\lambda}(r)\phi_{l,\lambda}(r)r^2\exp[(\epsilon_{l,\lambda}-\mu)/kT]\frac{r_b}{kT}\left[\frac{\partial\epsilon_{l,\lambda}}{\partial r_b}-\frac{\partial\mu}{\partial r_b}\right]}{\{\exp[(\epsilon_{l,\lambda}-\mu)/kT]+1\}^2},$$

$$T\dot{\mathcal{D}}(r_b,T,r/r_b)=2\sum_{l,\lambda}\frac{(2l+1)\phi^*_{l,\lambda}(r)T\frac{\partial\phi_{l,\lambda}(r)}{\partial T}r^2}{\exp[(\epsilon_{l,\lambda}-\mu)/kT]+1}-\sum_{l,\lambda}\frac{(2l+1)\phi^*_{l,\lambda}(r)\phi_{l,\lambda}(r)r^2\exp[(\epsilon_{l,\lambda}-\mu)/kT]\left[T\frac{\partial}{\partial T}(\epsilon_{l,\lambda}-\mu)+\mu-\epsilon_{l,\lambda}\right]}{kT\{\exp[(\epsilon_{l,\lambda}-\mu)/kT]+1\}^2}. \tag{A19}$$

Equation (A19) is written with the knowledge that $\phi_{l,\lambda}(r)$ is real. I have not yet programmed these equations for v' and $\dot v$, but rather I have used a finite difference method employing a variation of 1 part in 1000 in the temperature and the density.

APPENDIX B: CATALOG OF APPROXIMATIONS

The purpose of this appendix is to summarize in one place a list of the various approximations which are involved in my approach. As the problem addressed is rather complex, the list is long.

Throughout this paper, when there are well defined functions whose exact computation is somewhat lengthy, I have use Padé approximant representations which are typically accurate to within 0.1%.

My use of a cellular model does not take into account the variation in either size or shape of the cells which would be constructed by the Wigner-Seitz method of using planes which bisect the lines connecting each ion with its nearest neighbor ions.

In addition it is a further approximation to treat the ions as Maxwell-Boltzmann particles.

While it is exact for an ideal Fermi gas of chargeless electrons to use a Bravais lattice cellular model, I have made the further approximation to use spherical cells which incorporate the additional approximation that the ion is fixed at the center. However the center of mass motion is added to the pressure and the energies. The periodic boundary conditions, which were correct for the ideal Fermi gas, are used at every point on the surface of the spherical cell.

The Heitler-London Hamiltonian of the cellular model contains a term $-(i\hbar^2/m^*)\vec{k}\cdot\vec{\nabla}$. In spherical coordinates, this term, while diagonal in the z component of angular momentum, links every angular momentum component l with the $l+1$ and $l-1$ components. To reduce the very considerable computation effort which that feature entails, this term in the Hamiltonian is replaced by the sum of $+$ and $-$ the root mean square of its values in the appropriate ''nearly degenerate block.''

To go beyond the Heitler-London Hamiltonian adjustments are made to the potential in order to yield correct results in the limit as $y\to 0$. That is the approach to the ideal-gas limit. These adjustments are based on the idea that the electron density is uniform throughout the cell. However, while this feature is correct for both large and small de Broglie density ζ, the resultant electron-ion energy dips by about 6% when ζ is of the order of unity, which effect has not been accounted for.

The treatment of the exchange effects is also only approximate. I use a ζ dependent addition to the potential and an effective mass m^* which depends on both y and ζ when the two relevant electrons have parallel spins. The ion-ion exchange correction is neglected.

A further issue is how the corrections to the Heitler-London Hamiltonian should vanish in the limit as $y\to\infty$. I have used a semiclassical approximation to resolve this issue.

When I go beyond hydrogen, there are Z electrons in a cell with an ion of charge $+Ze$. This problem is currently intractable. As is well known the proper procedure is to integrate

$$\int \prod_{j=2}^{Z} d\vec{r}_j \langle \phi(\vec{r}_1,\ldots,\vec{r}_Z)|H-\mathcal{E}|\phi(\vec{r}_1,\ldots,\vec{r}_Z)\rangle = 0 \tag{B1}$$

which yields a Heitler-London-type equation for the $\vec{r}_1$ dependence of the wave function, but depends on a complicated potential. The same must be done for all the other electrons and a difficult self-consistency problem must be solved. Of course, the Hartree wave function is fine for the ion-electron interactions, but not so fine for the electron-electron interactions. Instead I make the independent electron model approximation. To this end I have introduced a self-consistent, density and temperature dependent potential. I compute this potential from the wave function through the use of Poisson's equation. As a further approximation, rather than removing the contribution for the wave function of the particular state being solved for, I simply remove a $1/Z$ fraction of the electron-electron interaction. These latter two approximations are the least well controlled and probably the most significant approximations made in this approach.

In addition to the approximations in the theory as described above, there are also numerical approximations as well. In particular, the number of mesh steps used in the radial coordinate is, of course, finite. There is as well the differencing scheme which is used in the numerical implementation of the Schrödinger equation, i.e., $(u_{i+1}+u_{i-1}-2u_i)/\Delta^2$. Together they limit the largest value that the kinetic energy can have. Also, both dv/dr and dv/dT are computed by a finite difference method instead of implementing the formulas of Appendix A. This method normally works well, but occasionally there are a different number of iterations involved between the quantities being differenced, which can sometimes cause a problem.

[1] G.A. Baker, Jr., Phys. Rev. E **56**, 5216 (1997).
[2] L.H. Thomas, Proc. Cambridge Philos. Soc. **23**, 542 (1927).
[3] E. Fermi, Rend. Accad. Naz. Lincei **6**, 602 (1927).
[4] R.P. Feynman, N. Metropolis, and E. Teller, Phys. Rev. **75**, 1561 (1949).
[5] E. Lieb, Rev. Mod. Phys. **53**, 603 (1981).
[6] R.G. Parr and W. Yang, *Density-Functional Theory of Atoms and Molecules* (Oxford University Press, New York, 1989).
[7] L. Spruch, Rev. Mod. Phys. **63**, 151 (1991).
[8] P.A.M. Dirac, Proc. Cambridge Philos. Soc. **26**, 376 (1930).
[9] R.D. Cowan and J. Ashkin, Phys. Rev. **105**, 144 (1957).
[10] P. Fromy, C. Deutsch, and G. Maynard, Phys. Plasmas **3**, 714 (1996).
[11] G.A. Baker, Jr. and J.D. Johnson, Physica A **265**, 129 (1999).
[12] K. Huang, *Statistical Mechanics* (Wiley, New York, 1963).
[13] N.W. Ashcroft and N.D. Mermin, *Solid State Physics* (Holt, Rinehart and Winston, New York, 1976).
[14] G.A. Baker, Jr. and J.D. Johnson, Phys. Rev. A **44**, 2271 (1991).
[15] H. Jeffreys and B.S. Jeffreys, *Methods of Mathematical Physics*, 2nd ed. (Cambridge University Press, London, 1950).
[16] L.D. Landau and E.M. Lifshitz, *Statistical Physics*, translated by E. Peierls and R.F. Peierls, Course of Theoretical Physics, Vol. 5 (Addision-Wesley, Reading, MA, 1958).
[17] H. Weingärtner and W. Schröer, Adv. Chem. Phys. **116**, 1 (2001).

[18] G.A. Baker, Jr. and J.D. Johnson, Phys. Plasmas **7**, 68 (2000).
[19] H.C. Graboske, Jr., D.J. Harwood, and F.J. Rodgers, Phys. Rev. **186**, 210 (1969).
[20] V.E. Fortov and V.K. Gryaznov, in *Strongly Coupled Plasma Physics*, edited by F.J. Rodgers and H.I. Dewitt (Plenum, New York, 1987), p. 87.
[21] See, for example, P.W. Anderson, *Concepts in Solids, Lectures on the Theory of Solids* (Benjamin, Reading, MA, 1963).
[22] G.A. Baker, Jr., J. Stat. Phys. **110**, 971 (2003).
[23] S. Eliezer, A. Ghatak, and H. Hora, *Fundamentals of Equations of State* (World Scientific, Singapore, 2002).
[24] C.E. Moore, *Ionization Potentials and Ionization Limits Derived from the Analyses of Optical Spectra, NSRDS-NBS 34* (National Bureau of Standards, Washington, 1970).